NOTICE: This is the author's version of a work that was accepted for publication in Computers & Geotechnics. Changes resulting from the publishing process, such as peer review, editing, corrections, structural formatting, and other quality control mechanisms may not be reflected in this document. Changes may have been made to this work since it was submitted for publication. A definitive version was subsequently published in Computers & Geotechnics, 155:105221, 2023. doi.org/10.1016/j.compgeo.2022.105221

Monopile installation in clay and subsequent response to millions of lateral load cycles

Patrick Staubach*; Lisa Tschirschky†; Jan Machaček‡; Torsten Wichtmann§

Abstract: The installation-induced changes in the state of clayey soils caused by pile driving processes are investigated numerically. Hydro-mechanically coupled Coupled-Eulerian-Lagrangian analyses are carried out for this purpose. After installation, the piles are subjected to one million lateral loading cycles using a novel high-cycle accumulation (HCA) model for clay implemented in an in-house code, modelling loading conditions to which piles are subjected in the offshore environment. Consistent with the results of field tests, it is found that higher values of initial overconsolidation ratio result in a greater increase in radial effective stress during the installation process. Compared to simulations neglecting the installation process, jacked piles show less accumulation of deformations when subjected to lateral cyclic loading, especially for a larger number of load cycles and for initially overconsolidated soil. It is concluded that the assumption of wished-in-place conditions is conservative in terms of pile rotation in most cases, while the stiffness of the soil-pile system at small rotations is comparable for jacked and wished-in-place piles.

Keywords: pile installation; high-cyclic loading; clay; high-cycle accumulation model; large deformations; offshore

1 Introduction

In current practice, the effects of the installation process of piles on their response to subsequent (lateral) loading are usually neglected in numerical studies. Recent numerical studies have investigated the influence of installation-induced changes in soil conditions for laterally loaded piles in sand by large-deformation finite element (FE) analysis (Heins and Grabe, 2017; Staubach et al., 2020; Bienen et al., 2021; Fan et al., 2021c; Le et al., 2021). In general, all studies concluded that the pile response is significantly altered by the installation process. In most cases, the current practice of neglecting the installation process (wished-in-place (WIP) conditions) leads to a less stiff response of the pile and to higher deformations when subjected to lateral or (in particular) vertical loads. In agreement with these findings, the results of centrifuge tests suggest that the consideration of the installation process leads to higher pile stiffness (Dyson and Randolph, 2001; Klinkvort, 2013; Fan et al., 2021b; Li et al., 2021).

Obviously, these trends do not necessarily apply to piles in clay, where it is to some extent unclear how the installation process will affect the pile's response to subsequent loading. It is also unclear whether

*Chair of Geotechnics, Bauhaus Universität Weimar, Germany/Chair of Soil Mechanics, Foundation Engineering and Environmental Geotechnics, Ruhr Universität Bochum, Germany. Email: patrick.staubach@uni-weimar.de, Corresponding author. ORCID: 0000-0002-1788-4880

†Chair of Soil Mechanics, Foundation Engineering and Environmental Geotechnics, Ruhr Universität Bochum, Germany/Chair of Geotechnics, Bauhaus Universität Weimar, Germany. ORCID: 0000-0002-1595-913X

‡Institute of Geotechnics, Technische Universität Darmstadt, Germany/Chair of Soil Mechanics, Foundation Engineering and Environmental Geotechnics, Ruhr-Universität Bochum, Germany. ORCID: 0000-0003-4849-5754

§Chair of Soil Mechanics, Foundation Engineering and Environmental Geotechnics, Ruhr-Universität Bochum, Germany. ORCID: 0000-0002-9250-7014

current practice, which assumes WIP conditions, is conservative or not. From field tests, in which primarily jacking was used as installation technique, it is known that the installation process changes the state of clayey soils considerably. During installation, an increase in (total) stresses and pore water pressure close to the open-ended pile tip occurs in clays (Lehane and Jardine, 1994a; Lehane and Jardine, 1994b). While installation in overconsolidated soils results in an increase in total and effective radial stresses at the tip (Bond and Jardine, 1991), there is little or no increase in effective radial stress at low values of initial overconsolidation ratio (OCR) (Lehane and Jardine, 1994b). For larger values of initial OCR, negative excess pore water pressures may develop near the pile shaft in greater distances from the pile tip (Bond and Jardine, 1991; Randolph, 2003). As the distance h of the soil from the pile tip increases (i.e. the pile is driven deeper into the soil), the total stress decreases. The change in the soil state with h is referred to as h/R effect (Karlsrud and Haugen, 1986; Coop and Wroth, 1989; Bond and Jardine, 1991; Lehane and Jardine, 1994a; Lehane and Jardine, 1994b), where h is normalised by the radius R of the pile. In contrast to the installation in sand (White and Lehane, 2004; Jardine et al., 2013), the h/R effect does not necessarily describe a reduction of effective radial stress with increasing h/R for piles in clay (Coop and Wroth, 1989; Lehane and Jardine, 1994a). The aforementioned effects during the installation process are schematically shown in Fig. 1, which qualitatively depicts results obtained from analyses presented later. As the pile tip passes ($h/R = 0$), the effective radial stress increases significantly, which is more pronounced at higher values of initial OCR. Once the pile tip has passed the soil, the effective radial stress reduces considerably in greater distance r/R from the pile shaft. Close to the pile shaft, however, negative excess pore water pressures (Δp^w) may develop, which leads to an increase in the effective radial stress. Larger negative excess pore water pressures are obtained for larger values of initial OCR.

After the installation is finished, the total stresses decrease, in particular close to the pile tip (Lehane and Jardine, 1994b). The change of the soil state with time following the installation is often referred to as equalisation or equilibration (Randolph, 2003). The dissipation of excess pore water pressure after installation results in an increase in effective radial stresses in normally consolidated or slightly overconsolidated clay once the consolidation process is complete (Lehane and Jardine, 1994b). In contrast, a reduction in effective radial stresses may occur in highly overconsolidated clay during the consolidation phase (Bond and Jardine, 1991; Lehane and Jardine, 1994a). Results of field tests comparing open and closed-ended piles indicate that the effective radial stresses are not influenced by the different pile configurations (Doherty and Gavin, 2011). So far, pile installation processes in clay have mainly been investigated using analytical or simplified numerical methods. Particularly noteworthy are the cavity expansion methods (see, for example, (Randolph et al., 1979; Lehane and Gill, 2004; Ali et al., 2011; Rezania et al., 2017; Cui et al., 2019; Gong et al., 2020)), which assume changes in soil state due to the installation process in radial direction only, and the strain path methods (see, for example, Baligh, 1985; Sagaseta et al., 1997; Xu et al., 2006; Ni et al., 2010), which additionally consider a dependence in vertical direction. Cavity expansion methods are known to predict unrealistic strain paths in the vicinity of the pile (Baligh, 1985), which is improved by the strain path method. De Chaunac and Holeyman, 2018 presented an approach using thin plane strain discs, modelling the soil with a rather sophisticated hypoplastic clay model and assuming ideally undrained conditions. Earlier application of FE techniques to the analysis of cone penetration tests, considering the "complete" installation process in one model, can be found in (Sheng et al., 2005). Recent studies of cone penetration tests in clay utilising particle FE techniques are reported in (Monforte et al., 2018; Hauser and Schweiger, 2021; Zhang et al., 2021). Rather sophisticated analyses of the installation of open-profile piles using the Coupled Eulerian-Lagrangian (CEL) method and assuming ideally undrained conditions are documented in (Chen et al., 2022). An alternative to using large-deformation schemes to investigate pile installation effects are the so-called Press-Replace techniques (Engin et al., 2015). However, similar to the cavity expansion methods, the soil flow around the pile tip is not fully captured.

Despite a large number of numerical studies on piles in clay subjected to lateral loading (see, for example, (Lin et al., 2016; Page et al., 2018; Zdravkovic et al., 2020)), the assumption of WIP conditions has never been shown to be justified, but has been adopted nevertheless. As mentioned in (Truong and Lehane, 2018), there is neither a comprehensive experimental nor a numerical study quantifying the influence of the installation process on the lateral loading behaviour of piles in clay. In centrifuge tests on

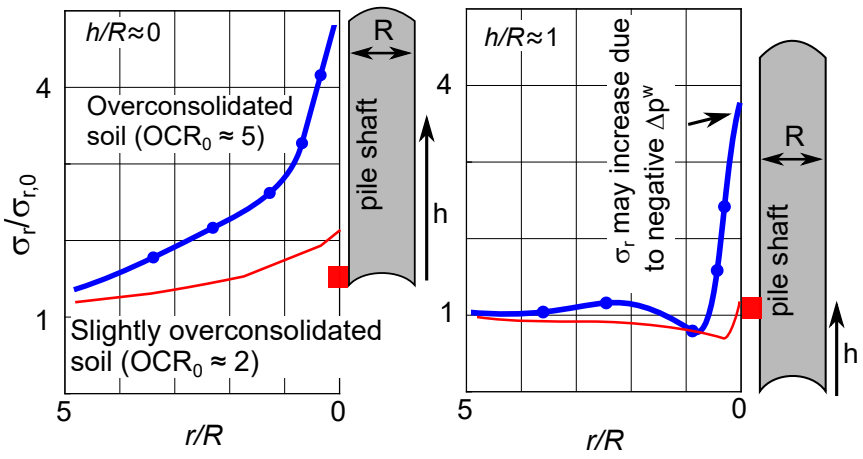

Figure 1: Schematic of the change in effective radial stress with respect to the normalised distance from the pile shaft r/R for different values of h/R

piles in clay, the installation is usually performed at 1 g (Hong et al., 2017; Yang et al., 2019; Lai et al., 2020; Kong et al., 2022), often justified by referring to earlier work adopting the same procedure. The installation at 1 g of course reduces the uncertainty, in particular relevant for numerical back-analysis of the tests (Duque et al., 2021), but does not reflect the processes taking place in reality. With regard to axially loaded piles, Randolph, 2003 argues that any approach predicting the shaft capacity of a driven pile must consider: (1) the installation-induced changes in the soil state, (2) the following dissipation of excess pore water pressure and (3) the load-induced changes in the soil state.

No attempt has yet been made to simulate the complete installation process of open-profile piles in clay considering partially drained conditions by solving the balance equations of mass of the soil-water mixture and linear momentum of the pore water phase (i.e. generation of excess pore water pressure and dissipation by consolidation is considered alongside effects resulting from inertia).

In this paper, the pile installation process by jacking and the subsequent (high-)cyclic lateral loading are numerically investigated. Lateral loading with a large number of load cycles is of particular importance for piles of offshore wind turbines (OWTs), which are subjected to millions of load cycles during the operational phase. This loading can lead to permanent deformation of the soil and thus to tilting of the structure, which must be within a narrow range of tolerable values. However, as mentioned above, it is unclear whether current practice, which neglects the installation process, leads to conservative results in terms of pile rotation. Furthermore, it is of interest whether long-term cyclic loading could completely erase the influence of the installation process, such that at a certain point in time it does not matter whether the installation is taken into account or not. The installation process is carried out using an extended CEL method considering partially drained conditions. This method allows to model the large soil movements during the installation process such that the full process can be modelled without any simplifications. After the installation, the state variables are transferred to a second, fully Lagrangian model. The consolidation process is considered before the lateral loading starts such that the aforementioned equalisation in the soil state may occur. The transfer is necessary since for the lateral loading a precise discretisation of the continuum using Lagrangian elements is beneficial and an implicit time integration scheme is required, whereas CEL methods usually adopt explicit time integration schemes. One million load cycles are then simulated using the high-cycle accumulation (HCA) model for clay (Wichtmann, 2016; Staubach et al., 2022b), which is a constitutive model specifically tailored to predict the mechanical response of clay to a large number of load cycles. In this paper, the HCA model is applied for the investigation of the long-term response of foundations for OWTs subjected to millions of load cycles for the first time. Up to now, no general continuum mechanics approach for the modelling of the response of piles in clay subjected to a large number of load cycles exists. The paper aims to close this gap in research.

2 Numerical analysis of the pile installation process in clay

2.1 Numerical model for the installation process

As mentioned in the introduction, an Eulerian FE technique is adopted in this work. In an Eulerian analysis, the mesh is fixed in space and the material moves through the mesh. Unlike a Lagrangian analysis, the elements are not necessarily fully occupied by material. An Eulerian approach is advantageous when large deformations are modelled since no mesh distortion occurs. In most Eulerian codes, a calculation increment is conceptually divided into two steps. In the first step, the solution is progressed in time analogous to a Lagrangian analysis. In the second step, the solution is then mapped back to the Eulerian mesh, which is called the *remap* or *advection* step. The strategy of solving the problem in two separate steps is often referred to as *operator split* since the underlying differential equations are solved term-by-term (see, for example, (Benson, 1992; Benson and Okazawa, 2004; Waltz, 2013; Aubram et al., 2015)). A method in which both Lagrangian and Eulerian elements are present and interact with each other is referred to as Coupled Eulerian-Lagrangian (CEL) method. In the commercial program package `Abaqus` the CEL method is implemented with an explicit time integration scheme. Successful applications of the CEL approach to geotechnical boundary value problems (BVPs) have been reported e.g. in (Qiu et al., 2011; Heins and Grabe, 2017). Based on the work of Hamann et al. (Hamann et al., 2015; Hamann, 2015), Staubach et al. (Staubach et al., 2021b) extended the CEL approach to hydro-mechanically coupled analyses, solving the balance of linear momentum of the soil-water mixture and the mass balance of the water simultaneously. Therefore, the displacement of the solid phase and the pore water pressure are spatially discretised, i.e. the **u**-p element formulation is used (Zienkiewicz et al., 1980). The **u**-p element formulation neglects the relative acceleration between the solid and the water phase. However, for soils with a low hydraulic conductivity, such as considered here, this assumption is valid (Zienkiewicz et al., 1980; Staubach and Machaček, 2019).

The numerical model is shown in Fig. 2. To consider relevant conditions for OWTs, piles with a diameter of $D = 4$ m are modelled, which might be judged as rather small dimensions considering piles being currently installed. However, with current numerical schemes only a limited penetration depth (8 m in the present case) can be simulated within reasonable time. Therefore, in order to consider realistic L/D ratios of monopiles, a smaller diameter is modelled. In line with this, a shallow water depth with the water level 10 m above the seabed is assumed. The total pore water pressure plays a vital role in the present analyses because effects resulting from cavitation are taken into account. The pile has a wall thickness of 0.08 m. The soil is discretised with Eulerian elements, while the pile is modelled with Lagrangian elements. To avoid artificial reflections of outward travelling waves at the fixed boundaries of the model, a distance of 80 m ($= 20D$) from the pile to the outer boundary and a height of the model of 200 m ($= 50D$) are chosen. The nodal spacing increases with increasing distance from the pile, resulting in a progressive loss of higher frequency waves. As can be seen from the acceleration field on the left-hand side of Fig. 2, the waves caused by the pile installation process do not reach the fixed boundaries of the model, proving that the results of the simulations are not altered by artificial reflections. As the installation process can lead to a heave of the soil surrounding the pile, an additional, initially material-empty volume above the seabed is considered (red area in Fig. 2). This additional volume can be filled with material during the installation process. The upper part of the model allows for drainage during installation by prescribing zero excess pore water pressure.

The Modified-Cam-Clay (MCC) model (Roscoe and Burland, 1968) is adopted as the constitutive model. The MCC model performs well for normally to lightly overconsolidated soils but overestimates the peak shear strength for more strongly overconsolidated clays (Mita et al., 2004). To resolve this issue, an additional failure surface, the Matsuoka-Nakai (Matsuoka and Nakai, 1974) bounding surface, is introduced in the MCC model. In the super-critical regime, the additional failure surface prevents the shear stress to reach unrealistic values. Since only monotonic jacking is considered as installation technique, the MCC model is considered sufficient to investigate the installation-induced changes in the soil state. Obviously, only unstructured clays can be studied using the standard MCC model. The MCC model is implemented by the authors using a radial-return mapping algorithm as proposed in (Borja and Lee, 1990).

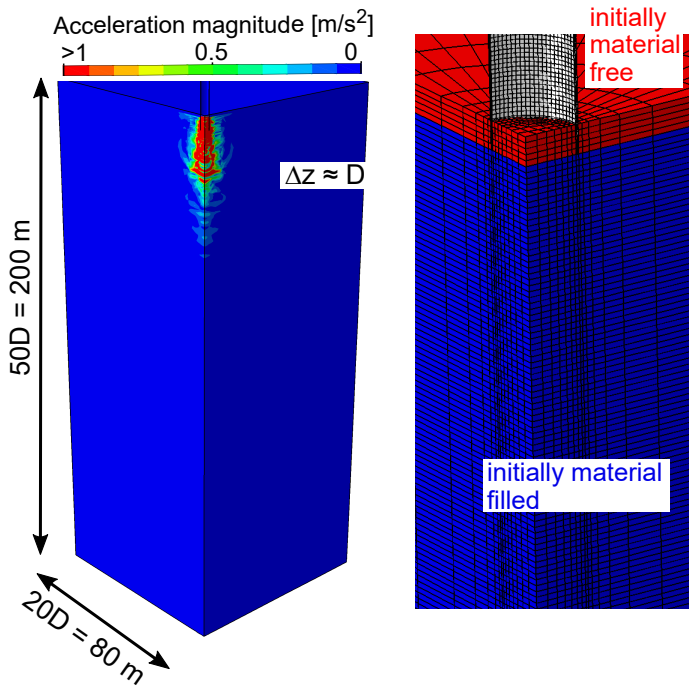

Figure 2: *Model for the simulation of the pile installation process and spatial distribution of the acceleration magnitude (gravity is subtracted) during the installation process at a pile penetration of approximately* $\Delta z = D$

"Karlsruhe kaolin" is considered as soil. "Karlsruhe kaolin" is chosen because the parameters of the HCA model for clay, introduced in Section 3.1, were determined for this material. "Karlsruhe kaolin" has a liquid limit $w_L = 47.2$ %, a plastic limit $I_P = 12.2$ % and a viscosity index $I_v = 1.5$ %. It is characterised in more detail in (Wichtmann, 2016). As shown in (Wichtmann, 2016; Staubach et al., 2022b), "Karlsruhe kaolin" shows almost no rate effects, which is due to the low value of I_v. Therefore, the application of the MCC model, which does not incorporate any strain rate dependence, is justified. The material properties of "Karlsruhe kaolin" for the MCC model are summarised in Table 1. The same critical stress ratio $M = 1$ ($\varphi_c = 25°$) is used for compression and extension, respectively.

Different values of initial OCR are studied by defining the pre-consolidation pressure p_c used in the MCC model. In overconsolidated soils, the initial stress state depends on OCR, via the lateral stress coefficient K_0 calculated as

$$K_0 = [1 - \sin(\varphi_c)] \cdot \mathrm{OCR}^{\sin(\varphi_c)}. \tag{1}$$

This relation has been proposed in (Mayne and Kulhawy, 1982) and has been applied in (Silva et al., 2006; Lehane et al., 2009) as well. A hydraulic conductivity of $k^w = 10^{-8}$ m/s is assumed. The installation is performed velocity controlled with a value of 0.3 m/s. The jacking velocity influences only the inertia forces and the consolidation. The jacking velocity is high compared to values typically found in practice, which is why effects resulting from inertia occur in the analyses. The accelerations close to the pile are approximately 2 m/s^2 in magnitude.

Note that the choice of the height of free water table is of great importance for the simulation of the installation in clay, since cavitation has to be accounted for. Numerically, cavitation is considered by the following equation:

$$\frac{n}{K^w}\dot{p}^w = \begin{cases} -\mathrm{div}\left\{\dfrac{K^{\mathrm{Perm}}}{\eta^w}\left[-\mathrm{grad}(p^w) + \rho^w\left(\boldsymbol{b} - \ddot{\boldsymbol{u}}^s\right)\right]\right\} - \mathrm{div}(\dot{\boldsymbol{u}}^s) & \text{if } p^w + \dot{p}^w\Delta t \geq -100 \text{ kPa} \\ 0 & \text{if } p^w + \dot{p}^w\Delta t < -100 \text{ kPa} \end{cases} \tag{2}$$

λ	κ	ν	M
0.13	0.05	0.3	1

Table 1: Material parameters of "Karlsruher kaolin" for the MCC model

Eq. (2) is essentially the mass balance of the pore water (Ehlers and Bluhm, 2013). Therein, n is the porosity, K^w is the bulk modulus of the pore water, $\dot{p}^w$ is the rate of pore water pressure, K^{Perm} is the permeability of the soil, η^w is the dynamic viscosity of the water, p^w is the pore water pressure relative to the atmospheric pressure (assumed to be 100 kPa), ρ^w is the density of water, $\boldsymbol{b}$ is the gravity vector, $\ddot{\boldsymbol{u}}^s$ is the acceleration of the solid phase, $\dot{\boldsymbol{u}}^s$ is the velocity of the solid phase and Δt is the time increment. As is visible from Eq. (2), the change of pore water pressure is zero if adding the current increment of pore water pressure would lead to cavitation. Eq. (2) is implemented in the VUMAT subroutine used for the hydro-mechanically coupled CEL method.

2.2 Results of the simulations of the pile installation process

In Fig. 3a the pile penetration versus the jacking force is shown for different initial OCR values. All four simulations are performed assuming frictionless contact ($\mu = 0$) and a water level above the seabed of $H^w = 10$ m. Frictionless contact is preferred due to improved numerical stability and accuracy. As expected, the higher the initial value of OCR, the higher is the jacking force required to reach the targeted penetration depth. A comparison with a simulation considering a friction coefficient of $\mu = 0.25$ for an initial OCR of 3 is shown in Fig. 3b. The influence of the friction of the pile shaft is rather small, which justifies the use of a frictionless contact for this value of initial OCR. The reason for the low influence of friction is that the normal contact stress at the pile shaft is very low for greater vertical distances from the pile tip due to negative excess pore water pressures allowing for a "free standing height" of the soil without needing the pile as support (no earth pressure). This is particular the case for the simulations with a higher initial value of OCR. Results of a numerical study (not presented in this paper) indicate that the influence of friction is more pronounced in case of $\text{OCR}_0 = 1$. In this special case the assumption of frictionless contact becomes questionable, but was adopted nevertheless in order to allow for a clear comparison with the other simulations. To investigate the influence of cavitation, Fig. 3c depicts the results of a simulation where the water table is assumed to be at ground surface level ($H^w = 0$ m) for an initial OCR of 6. Since the negative excess pore water pressure can reach smaller values in the case of $H^w = 10$ m compared to $H^w = 0$ m, a higher pile resistance is observed for $H^w = 10$ m.

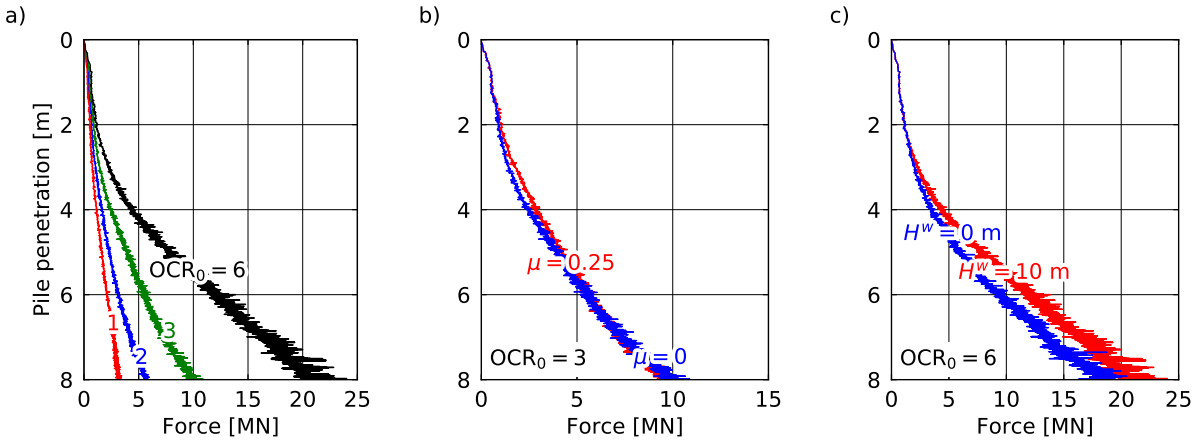

Figure 3: *Pile penetration vs. jacking force for different values of initial OCR (a), different values of friction coefficient μ (b) and different heights H^w of water table above the seabed (c)*

The spatial distributions of excess pore water pressure, effective radial stress and OCR are shown in Fig. 4 for initial values of OCR of $\text{OCR}_0 = 2$ and $\text{OCR}_0 = 6$. Note that the geotechnical sign convention

is used for the effective radial stress. For $OCR_0 = 6$, a much larger area with negative excess pore water pressures is observed at the pile shaft. In addition, slightly larger positive excess pore water pressures are generated below the pile tip. The soil inside the pile tends to move downwards with the pile in the case of $OCR_0 = 6$, which is not the case for $OCR_0 = 2$. This is due to the aforementioned negative excess pore water pressure. Large differences between the two simulations are also observed for the field of effective radial stress. In the case of $OCR_0 = 6$, much higher values occur near the pile. While the effective stress below the pile tip is reduced for the lower value of the initial OCR, opposite trends are observed for the higher initial OCR. The higher values of effective radial stress and negative excess pore water pressure are not unexpected considering that the jacking force given in Fig. 3a is also much higher for $OCR_0 = 6$. Due to the larger negative excess pore water pressure at the pile shaft for $OCR_0 = 6$, the effective radial stress at the pile shaft increases much more compared to the simulation assuming $OCR_0 = 2$. However, for a larger distance from the pile shaft, both simulations show a strong decrease of the effective radial stress compared to the initial value (h/R effect). The reduction of the radial stress with increasing h/R is more pronounced in the case of $OCR_0 = 2$. For the installation of piles in sand (White and Lehane, 2004; White and Bolton, 2004; Jardine et al., 2013; Yang et al., 2020), the negative excess pore water pressures tend not to be as large as in clay (or are not existent at all), for why the effective radial stress is lowest at the pile shaft. This is not the case for an installation in clay, where in particular the simulation with a higher initial value of OCR shows large values of effective stress at the pile shaft due to negative excess pore water pressure. This is in line with the general trend observed in field tests (Bond and Jardine, 1991; Randolph, 2003) and results from the tendency of the overconsolidated soil to show dilatant behaviour when subjected to shearing in the super-critical regime. The spatial distribution of OCR shows that the installation process drastically reduces the initial OCR below the pile tip for both the initially slightly overconsolidated ($OCR_0 = 2$) and the initially more overconsolidated ($OCR_0 = 6$) soil. This is due to the fact that the mean effective stress increases significantly below the pile tip for both simulations, particularly the vertical component of the effective stress tensor. In agreement with the observed effective stress ratios at the pile shaft, larger OCR values relative to the initial values are observed for $OCR_0 = 2$ as the effective stresses decrease. This is less pronounced in the simulation with $OCR_0 = 6$, which is due to the larger negative excess pore water pressures already mentioned.

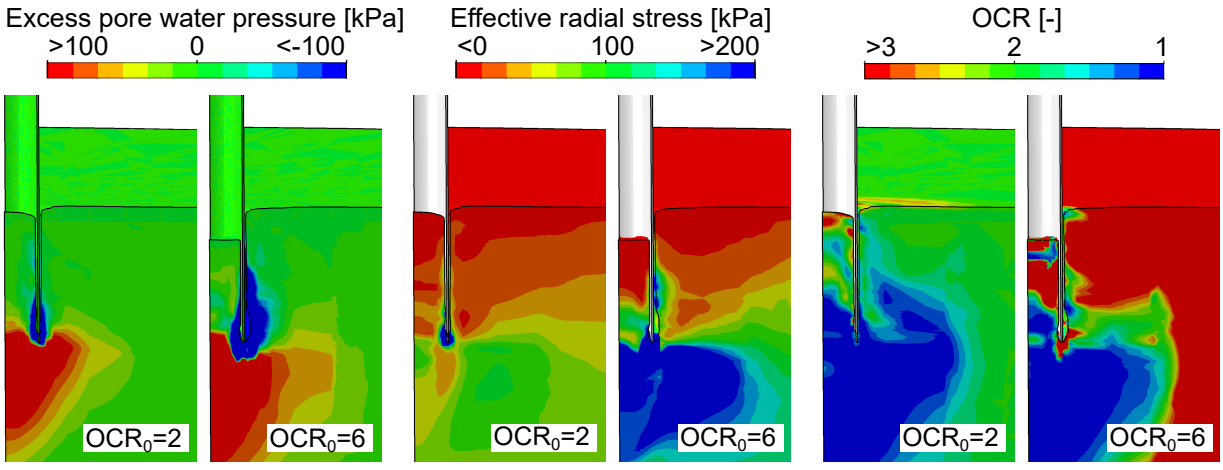

Figure 4: *Spatial distributions of excess pore water pressure, effective radial stress and OCR at a pile penetration depth of 8 m for an initial OCR of $OCR_0 = 2$ and $OCR_0 = 6$, respectively*

Plots of the normalised effective radial stress $\sigma_r/\sigma_{r,0}$ and normalised excess pore water pressure p^w/p_0^w (including the pressure from the free water table $H^w = 10$ m above the seabed) with distance to the (outer) pile shaft for a depth of 5.2 m below the seabed are given for different values of h/R in Fig. 5 for initial values of $OCR_0 = 2$ and $OCR_0 = 6$. For each value of h/R, the spatial distribution of effective radial stress for $OCR_0 = 2$ is given. In addition, the line along which $\sigma_r/\sigma_{r,0}$ and p^w/p_0^w are evaluated is depicted in Fig. 5.

When passing the pile tip ($h/R = 0$), the effective radial stress increases significantly at greater distance

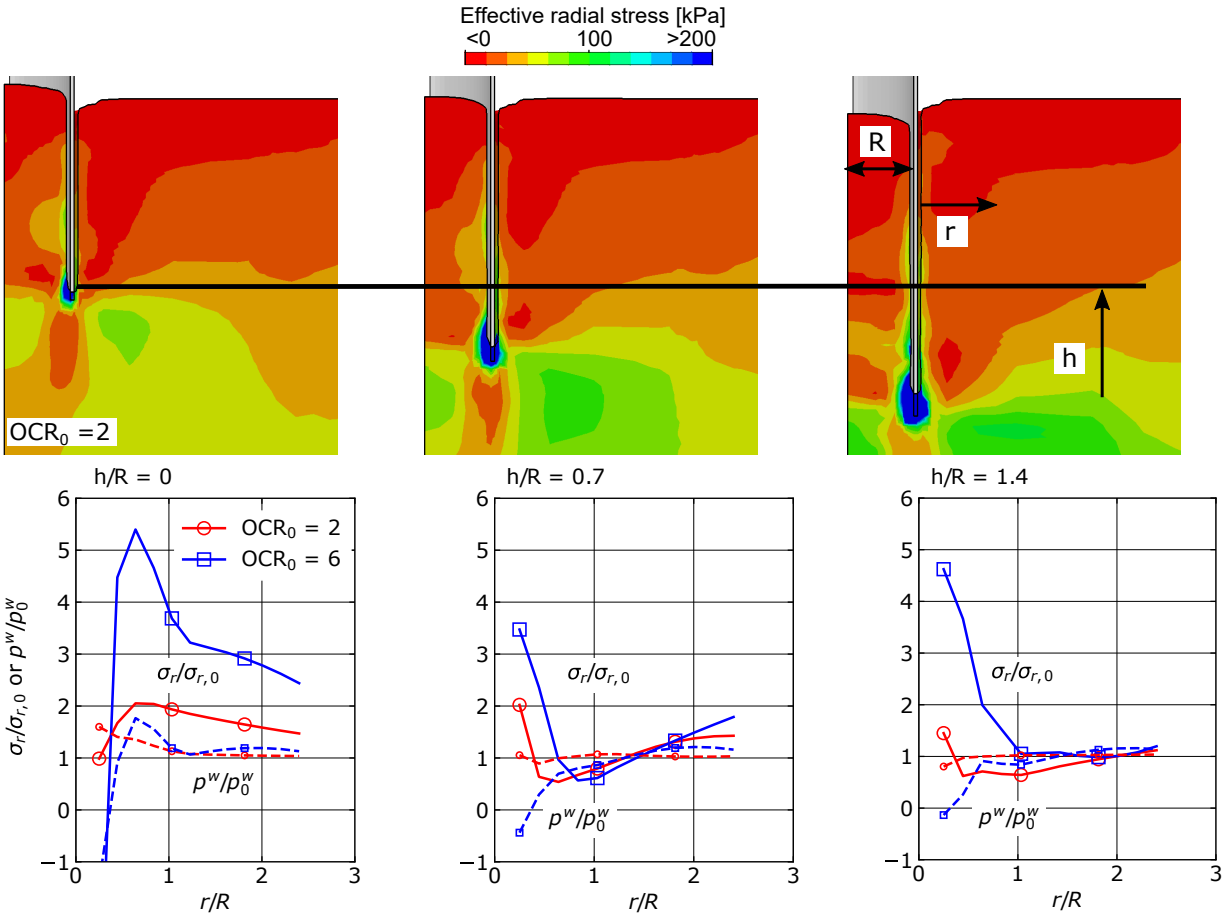

Figure 5: *Spatial distribution of effective radial stress and corresponding plots of normalised effective radial stress $\sigma_r/\sigma_{r,0}$ (solid) and normalised excess pore water pressure p^w/p_0^w (dashed) vs. normalised radial distance r/R from the pile shaft in a depth of 5.2 m at different values of h/R for an initial OCR of $OCR_0 = 2$ and $OCR_0 = 6$*

from the pile shaft for both initial values of OCR. In the immediate vicinity, however, there is a sharp decrease, which is limited to a very small soil zone. At greater distances from the pile tip, values greater than the initial effective radial stress are reached, which is more pronounced in the case of the simulation with a higher initial OCR. In the case of $\mathrm{OCR}_0 = 6$, the trend of the normalised pore water pressure p^w/p_0^w is qualitatively very similar to that of the effective radial stress. For $\mathrm{OCR}_0 = 2$ and for larger values of h/R, opposite trends are observed, as can be seen from the plots for $h/R = 0.7$. For this depth, both simulations show qualitatively similar trends for both the effective radial stress and the excess pore water pressure. As observed earlier, the higher initial OCR value leads to higher negative pore water pressures and thus higher effective radial stresses near the pile shaft. This tendency is also obtained using the strain path method (De Chaunac and Holeyman, 2018). At greater distance from the pile shaft, almost no excess pore water pressures occur in either simulation and the effective radial stress decreases from $h/R = 0$ to $h/R = 0.7$. The decrease with increasing distance from the pile continues as pile penetration progresses, as can be seen from the diagram for $h/R = 1.7$. While in the simulation with $\mathrm{OCR}_0 = 2$ the values of the effective radial stress are almost identical to the initial values even near the pile shaft, the effective radial stress near the pile shaft continues to increase in the case of $\mathrm{OCR}_0 = 6$. This increase occurs despite a decrease in the negative excess pore water pressures. Figure 5 also demonstrates that the h/R effect will influence the lateral response of the pile considering that the stresses are changing with h/R even in a distance $r/R > 1$.

Compared to the pile installation process in sand, where the effective radial stress tends to decrease near the pile shaft with increasing h/R, piles in clay show an opposite tendency, especially for higher

values of initial OCR. This is consistent with research reported in (Lehane and Jardine, 1994b; Bond and Jardine, 1991; Lehane and Jardine, 1994a) which found higher effective stresses for higher values of initial OCR prior to installation.

3 High-cyclic lateral loading following the installation process

3.1 The HCA model for clay

For a simulation with a very large number of loading cycles, the calculation of each individual cycle is not useful as it leads to an accumulation of numerical errors and the computational effort becomes very large (Niemunis et al., 2005). Therefore, when calculating with a high-cycle accumulation (HCA) model, only the trend of the deformation with increasing number of cycles is predicted. The different calculation strategies are schematically shown in Fig. 6. For calculations with the HCA model, the cyclic strain amplitude, retrieved from the strain path of a single load cycle, calculated with a conventional constitutive model, is required as input. Typically, two single load cycles are simulated with a conventional constitutive model, of which the second cycle is used to record the strain path, from which the strain amplitude is calculated. This is schematically shown in Fig. 6b. During the high-cycle mode, the strain amplitude is a function of the soil stiffness using a so-called adaptive strain amplitude definition (Staubach et al., 2022a), which takes into account changes in stiffness caused by the cyclic loading. Therefore, so-called update cycles, which are used to update the strain amplitude simulating an individual load cycle at some point during the high-cycle phase, are not necessary. Details on the procedure adopted by the adaptive strain amplitude definition can be found in Appendix A.

The HCA model for sand by (Niemunis et al., 2005) is an established model for the analysis of a large number of load cycles (see, for example, (Zachert et al., 2020; Jostad et al., 2020; Page et al., 2021; Le et al., 2021)). The recently proposed HCA model for clay (Wichtmann, 2016; Staubach et al., 2022b) is based on data from an extensive laboratory testing program on kaolin under undrained cyclic loading (Wichtmann and Triantafyllidis, 2018) and adopts the general framework of the HCA model for sand.

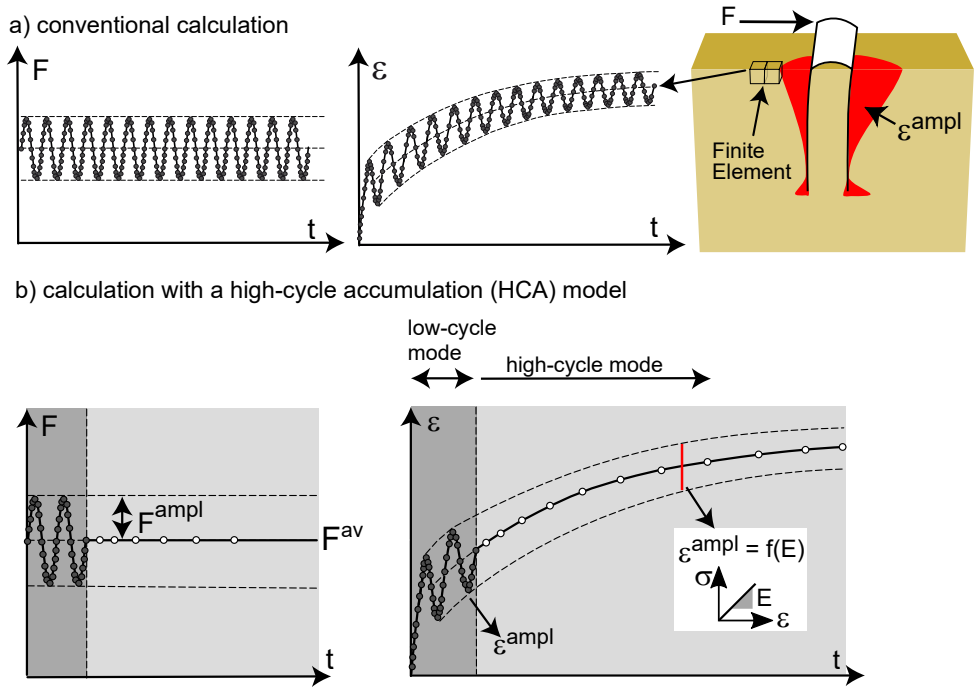

Figure 6: *Calculation strategy in conventional analyses and in simulations using the HCA model*

Both HCA models utilise the same basic, elasto-plastic, stress-strain rate relationship given by

$$\mathring{\boldsymbol{\sigma}} = \mathsf{E} : (\dot{\boldsymbol{\varepsilon}} - \dot{\boldsymbol{\varepsilon}}^{\mathrm{acc}} - \dot{\boldsymbol{\varepsilon}}^{\mathrm{pl}}). \tag{3}$$

Therein, the (objective) stress rate $\mathring{\boldsymbol{\sigma}}$ of the effective Cauchy stress $\boldsymbol{\sigma}$ (compression positive), the strain rate $\dot{\boldsymbol{\varepsilon}}$ (compression positive), the accumulation rate $\dot{\boldsymbol{\varepsilon}}^{\mathrm{acc}}$, a plastic strain rate $\dot{\boldsymbol{\varepsilon}}^{\mathrm{pl}}$ (necessary only for stress paths touching the yield surface) and the pressure-dependent elastic stiffness E. In the context of HCA models, the dot above a symbol denotes a derivative with respect to the number of cycles N, i.e. $\dot{\square} = \partial \square / \partial N$. In transient analyses, i.e. analyses performed in physical time, the integration of Eq. (3) is performed using $\Delta N = \Delta t / t_{\mathrm{cycle}}$, where Δt is the time increment applied by the FE program and t_{cycle} is the duration of a single cycle.

The key aspect of the HCA models is the accumulation rate $\dot{\boldsymbol{\varepsilon}}^{\mathrm{acc}}$, which corresponds to the permanent strain due to the cyclic loading. For the HCA model for clay, $\dot{\boldsymbol{\varepsilon}}^{\mathrm{acc}}$ is calculated by the following multiplicative approach

$$\dot{\boldsymbol{\varepsilon}}^{\mathrm{acc}} = \dot{\varepsilon}^{\mathrm{acc}}\, \mathbf{m} = f_{\mathrm{ampl}}\; \dot{f}_N\; f_e\; f_\eta\; f_{\mathrm{OCR}}\; f_f\; \mathbf{m}. \tag{4}$$

The factors $f_\square$ of the intensity of accumulation $\dot{\varepsilon}^{\mathrm{acc}}$ take into account the influence of the strain amplitude $\varepsilon^{\mathrm{ampl}}$ (f_{ampl}), the cyclic preloading ($\dot{f}_N$, using the preloading variable g^A which weights the number of applied cycles N by the strain amplitude $\varepsilon^{\mathrm{ampl}}$ of these cycles), the average void ratio e^{av} (f_e), the average stress ratio η^{av} (f_η), the average overconsolidation ratio $\mathrm{OCR}^{\mathrm{av}}$ (f_{OCR}) and the loading frequency f (f_f). $\mathbf{m}$ is the direction of accumulation (unit tensor), analogous to the direction of plastic strain in conventional elasto-plastic models. The functions and corresponding material constants are given in Table 2. Since "Karlsruhe kaolin" shows almost no strain rate effects, the function f_f is equal to one. An overview of the complete model including the derivation of the constitutive equations, the determination of the parameters and the simulation of element tests is given in (Wichtmann, 2016; Staubach et al., 2022b). Because the model is formulated in terms of effective stresses, and the factors in Eq. (4) depend on the change of effective stress, the HCA model is also suitable for analyses with partially drained conditions.

Function	Material constant	Ref. quant.
$f_{\mathrm{ampl}} = \left(\dfrac{\varepsilon^{\mathrm{ampl}}}{\varepsilon^{\mathrm{ampl}}_{\mathrm{ref}}} \right)^{C_{\mathrm{ampl}}}$	C_{ampl}	$\varepsilon^{\mathrm{ampl}}_{\mathrm{ref}}$
$\dot{f}_N = \dot{f}_N^A + \dot{f}_N^B$ $\dot{f}_N^A = C_{N1} C_{N2} \exp\left[-\dfrac{g^A}{C_{N1} f_{\mathrm{ampl}}} \right]$ $\dot{f}_N^B = C_{N1} C_{N3}$ $\dot{g}^A = \dot{f}_N f_{\mathrm{ampl}}$	C_{N1} C_{N2} C_{N3}	
$f_e = \dfrac{(C_e - e^{\mathrm{av}})^2}{1 + e^{\mathrm{av}}} \dfrac{1 + e_{\mathrm{ref}}}{(C_e - e_{\mathrm{ref}})^2}$	C_e	e_{ref}
$f_\eta = \exp\left(C_\eta \, \lvert\eta^{\mathrm{av}}\rvert / M \right)$	C_η, M	
$f_{\mathrm{OCR}} = \exp[-C_{\mathrm{OCR}}(\mathrm{OCR}^{\mathrm{av}} - 1.0)]$	C_{OCR}	
$f_f = 1$	-	

Table 2: Functions, material constants and reference quantities of the HCA model for clay (Wichtmann, 2016; Staubach et al., 2022b)

Eq. (3) incorporates a plastic strain rate to avoid the stress state to reach un-physical values during the high-cyclic loading (e.g. far outside the failure locus). The isotropic yield surface of the MCC model

C_{ampl}	C_{N1}	C_{N2}	C_{N3}	C_e	C_η	C_{OCR}
0.8	0.00125	0.5	0.0	-0.97	2.9	0.5

Table 3: Adopted HCA clay parameters for "Karlsruhe kaolin"

is used, which is given by

$$F = p^{\text{av}}(p^{\text{av}} - p_e^{\text{av}}) + \left(\frac{q^{\text{av}}}{M}\right)^2 \leq 0, \tag{5}$$

with the average mean effective stress p^{av}, the average deviatoric stress q^{av} and the average value of equivalent pressure p_e^{av}. The average overconsolidation ratio during the high-cycle phase is calculated by

$$\text{OCR}^{\text{av}} = \frac{p_e^{\text{av}}}{p_e^+}. \tag{6}$$

p_e^+ is calculated from Eq. (5) enforcing $F = 0$, viz.

$$p_e^+ = p^{\text{av}}\left[1 + \left(\frac{q^{\text{av}}}{M\ p^{\text{av}}}\right)^2\right]. \tag{7}$$

An isotropic stiffness is used for E in Eq. (3), which is defined by

$$\mathsf{E} = K\mathbf{1} \otimes \mathbf{1} + 2G\mathsf{I}, \tag{8}$$

where the scalar factors are given by

$$K = \frac{1 + e^{\text{av}}}{\kappa} p^{\text{av}} \quad \text{and} \quad G = \frac{3K(1 - 2\nu)}{2(1 + \nu)}. \tag{9}$$

In Eq. (9), ν is the Poisson's ratio and e^{av} is the average void ratio. $\mathbf{1}$ in Eq. (8) is the second-order unit tensor and I is the fourth order unit tensor.

The flow rule of the MCC model is chosen as direction of the accumulation $\mathbf{m}$. It is given by

$$\mathbf{m} = \left[\frac{1}{3}\left(p^{\text{av}} - \frac{(q^{\text{av}})^2}{M^2 p^{\text{av}}}\right)\mathbf{1} + \frac{3}{M^2}(\boldsymbol{\sigma}^{\text{av}})^*\right]^{\rightarrow}, \tag{10}$$

where $(\boldsymbol{\sigma}^{\text{av}})^* = \boldsymbol{\sigma}^{\text{av}} - \text{tr}(\boldsymbol{\sigma}^{\text{av}})/3\ \mathbf{1}$ denotes the deviatoric part of the average stress tensor and $\sqcup^{\rightarrow} = \sqcup / \| \sqcup \|$ the normalisation. The suitability of this definition for $\mathbf{m}$ has been shown in (Wichtmann, 2016; Wichtmann and Triantafyllidis, 2018).

The model has been validated for the range of magnitudes of soil state variables (OCR, stress ratio and mean effective stresses) considered in this paper. In addition, the back-analysis of a centrifuge test on monopiles subjected to cyclic lateral loading under partially drained conditions (cyclic loading frequency of 0.2 Hz in model scale and hydraulic conductivity of approximately $2 \cdot 10^{-6}$ m/s at 100 g) showed a good performance of the HCA model for clay (Staubach et al., 2022b). The parameters of "Karlsruhe kaolin" for the HCA model for clay have been determined based on a large number of undrained cyclic triaxial tests documented in (Wichtmann, 2016). They are given in Table 3. The reference values are $\varepsilon_{\text{ref}}^{\text{ampl}} = 10^{-3}$ and $e_{\text{ref}} = 1.25$.

3.2 Numerical model for the high-cyclic loading

A schematic representation of an offshore wind turbine founded on a monopile is shown in Fig. 7a. The load due to wind and water waves is assumed to act at identical frequency, so it is sufficient to consider

only a total horizontal force acting 8 m above the seabed. The adopted FE model is given in Fig. 7b. Initial sensitivity analyses on the required fineness of the mesh confirmed that the adopted model results in mesh-independent results. The field of excess pore water pressure following the installation with an initial OCR of 3 is depicted.

To investigate the long-term behaviour of the piles after installation, the FE program `numgeo`[1] is used. The HCA model for clay is implemented in `numgeo`. Since comparatively small deformations occur and high accuracy of the numerical solution is required, a fully Lagrangian FE model with implicit time integration is used for the analyses. For the soil, three-dimensional **u**-p finite-elements with 27 nodes are used to discretise the displacement **u** of the solid phase and 8 nodes to discretise the pore water pressure p^w. Standard (tri-)quadratic Lagrangian interpolation functions for the solid displacement and linear interpolation functions for the pore water pressure are used (i.e. Taylor-Hood element formulation (Taylor and Hood, 1973)). During the analyses, all boundaries of the model except the symmetry-plane allow for the dissipation of any excess pore water pressures.

For the pile, 27-noded single-phase elements are used, which are well suited for the analysis of bending of stiff materials. The pile is modelled elastically, with a stiffness of 210 GPa and a Poisson's ratio of 0.3. An extension of 5 cm above the seabed is considered, which is modelled with a stiffness 1000-times higher to distribute the concentrated loads acting on the pile head. The bending moment M^{tot} (see Fig. 7b) is applied as a pair of vertical forces acting in opposite direction on two nodes lying on the symmetry plane. The contact between the soil and the pile is discretised using an element-based mortar contact discretisation method with nine integration points per FE surface. The implementation of the mortar technique in `numgeo` is discussed in detail in (Staubach et al., 2022c). The penalty method is used to enforce the normal contact constraint. In `numgeo`, the penalty factor is determined based on the stiffness of the material adjacent to the contact and is 30-times the trace of the stiffness tensor. A simple Coulomb friction model with a friction coefficient of $\mu = 0.25$ and a dilatancy angle of zero is used. Typically, however, the friction coefficient has only very limited influence on the response of piles to lateral loading (Klinkvort, 2013). Creation of a normal gap between the soil and the pile is prohibited, as long as no cavitation occurs. Since a water level of 10 m above the seabed is assumed for all simulations, no cavitation and hence no opening of the soil-pile interface was observed in any analysis. The analyses are performed geometrically non-linear, using the Zaremba-Jaumann stress rate to ensure the objectivity of the stress rate. The Hughes-Winget algorithm is used to integrate the stress rate (Hughes and Winget, 1980).

The state variables, i.e. the void ratio, the OCR (by means of the pre-consolidation pressure), the effective stress tensor and the excess pore water pressure of the soil after installation are imported into the Lagrangian model by a nearest neighbour search of the integration points of both models. The same mapping procedure as in (Heins and Grabe, 2017; Staubach et al., 2020; Fan et al., 2021a) is used. The nearest neighbour search is performed for each of the 27 integration points of the `u27p8` elements individually. Note that the deformation of the soil is not transferred, as its influence is considered insignificant compared to the influence of the change in state variables. In addition to the previously mentioned studies, the excess pore water pressure is transferred to the Lagrangian model.

In addition to the simulations that take into account the installation-related soil changes, WIP simulations are carried out (no consideration of installation effects, i.e. current practice). For these analyses, a constant density, a K_0-stress state and a hydrostatic pore water pressure distribution are assumed. The same relationship between initial OCR and K_0 given by Eq. (1) is used.

In case of the simulations considering the installation-induced soil changes, the consolidation process prior to lateral loading is taken into account as it is assumed that there is sufficient time for the excess pore water pressure to dissipate between the installation of the piles and the start of use of the structure. Lateral loading begins as soon as hydrostatic conditions are reached. This assumption can be questioned, since for a hydraulic conductivity of $k^w = 10^{-8}$ m/s, it takes about 25 days for most of the excess pore water pressure to dissipate in the case of $\mathrm{OCR}_0 = 3$. The average time to install the pile and turbine of the

[1] `numgeo` (Machaček & Staubach, see (Machaček, 2020; Machaček and Staubach, 2021; Machaček et al., 2021; Staubach et al., 2021a; Staubach et al., 2022b; Staubach et al., 2021c; Staubach et al., 2021b; Staubach et al., 2022a) and `www.numgeo.de`) is a stand-alone FE program developed by the third and first author to solve nonlinear coupled (dynamic) geotechnical boundary value problems.

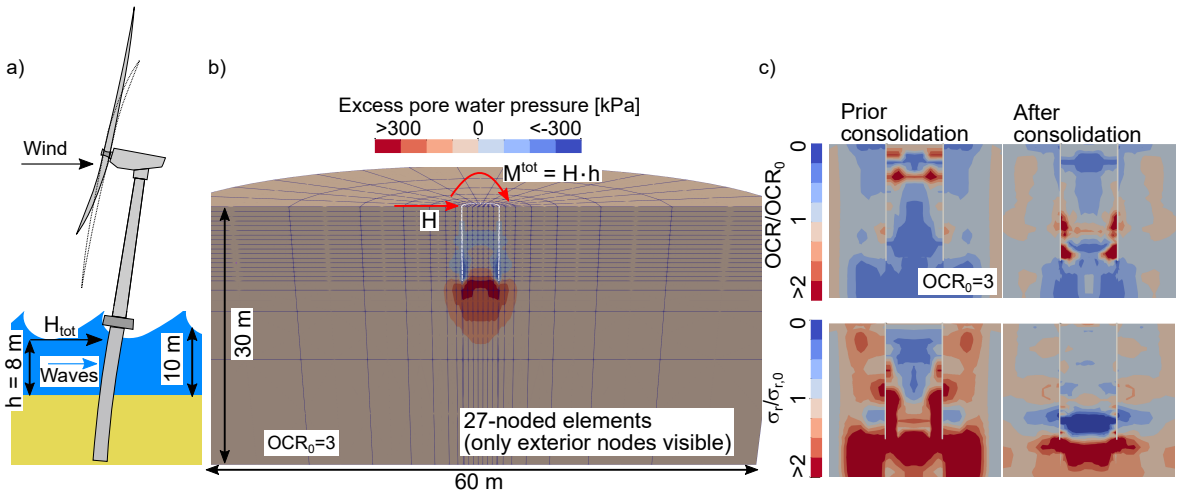

Figure 7: *a) Schematic of an offshore wind turbine and assumed lever arm h of the combined horizontal force of wind and water waves. b) Numerical model to analyse the lateral loading of the pile after installation and the transferred spatial distribution of the excess pore water pressure after jacking with an initial OCR of 3. c) Spatial distributions of normalised OCR and normalised horizontal effective stress $\sigma_r/\sigma_{r,0}$ before and after the consolidation process for the jacked pile with $OCR_0 = 3$.*

offshore wind turbine in reality is about 5 days (Lacal-Arántegui et al., 2018). Therefore, the pile could be loaded by wind and water waves before the hydrostatic conditions are reached. Such a scenario is not considered in order to allow a clear comparison with the WIP simulations, which also assume hydrostatic conditions.

3.3 Monotonic lateral loading following the installation

Prior to the simulations considering high-cyclic loading, monotonic load tests are performed to determine the maximum moment resistance of the piles with different initial OCR values. The following steps are performed:

1. After transferring the void ratio, effective stress and excess pore water pressure, a consolidation analysis is performed before loading the pile. $2 \cdot 10^6$ s $\approx$ 25 days are considered, which is sufficient time for the dissipation of all excess pore pressure. The soil-pile system is allowed to deform such that static force equilibrium is achieved. This is necessary because the system is not in static force equilibrium at the end of the installation process due to inertial forces (close to the pile, acceleration magnitudes of approximately 2 m/s^2 exist at the end of the installation process). As a result, the soil shows a maximum displacement of $\approx$ 5 mm in this calculation phase. For the WIP simulation, only the contact between pile and soil is initialised in this step.

2. The pile is loaded vertically with a magnitude of 0.2 MN to account for the weight of the structure supported by the pile. Compared to the vertical loads in real wind farms, this load is rather small, even if the lower embedment length is accounted for. This is because in the WIP simulations, larger values of vertical load lead to very large vertical displacements of up to 1 m for $OCR_0 = 1$, indicating a failure of the pile that cannot be modelled with a fully Lagrangian model. This is not the case for the jacked pile, where only small vertical displacements are observed ($\approx$ 4 cm for the jacked pile vs. $\approx$ 40 cm for the WIP simulation in case of $OCR_0 = 1$ and a load of 0.2 MN). These results already demonstrate the importance of considering the installation process, since the application of a realistic vertical load is not possible in case of the WIP simulations.

3. The moment applied at seabed level, see Fig. 7a, is linearly increased until a rotation of 4° is reached at the pile head. Assuming a lever arm of 8 m, the horizontal load is increased linearly

at the same time. This step is carried out either assuming ideally drained conditions or partially drained conditions with a hydraulic conductivity of $k^w = 10^{-8}$ m/s. In the latter case, the loading required for a pile head rotation of 2° is approximately reached at 10 s of loading, resulting in nearly ideally undrained conditions during loading.

In analogy to the simulation of the installation process, the MCC model and the parameters of "Karlsruhe kaolin" are utilised for these steps.

Figure 7c shows the spatial distributions of normalised OCR ($\mathrm{OCR}/\mathrm{OCR}_0$) and normalised horizontal effective stress $\sigma_r/\sigma_{r,0}$ before and after the consolidation phase performed in step 1 for the simulation assuming an initial OCR of 3. The fields before consolidation correspond to the transferred fields from the installation simulation. The consolidation process changes both fields significantly. As the negative excess pore water pressure dissipates at the pile shaft, the effective radial stress decreases, leading to an increase in OCR, especially inside the pile. At greater distances from the pile shaft, values greater than $\mathrm{OCR}_0 = 3$ are also achieved. In addition, an increase in OCR below the pile tip is observed. Here, two opposing effects are at work, namely the increase in effective stress due to dissipation of the positive excess pore water pressure and the decrease of the effective stress due to the unloading of the pile by releasing the jacking force. Apparently, the second effect outweighs the first. Figure 7c shows that strong installation-induced changes in the soil state are present even after consolidation is completed.

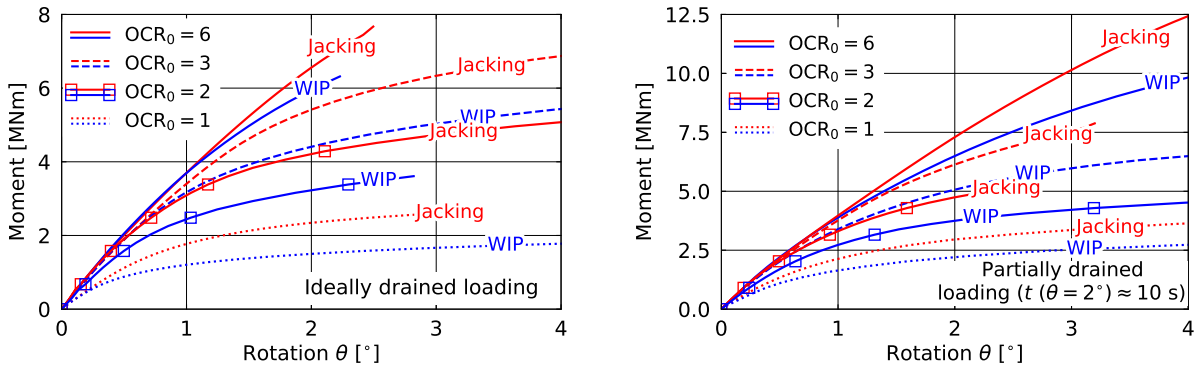

Figure 8: *Comparison of moment vs. rotation plots of jacked and WIP piles assuming ideally drained conditions (left-hand plot) and partially drained conditions (right-hand plot), respectively, for different values of initial OCR (moments are given for a full 3D model)*

The results of the monotonic load tests are shown in Fig. 8. Two different loading scenarios are investigated. Either the load is increased linearly, assuming ideally drained conditions (left-hand plot) or partially drained conditions (right-hand plot). Note that some simulations do not converge when the load is increased further, which is why not all results are shown up to a rotation of 4°. Not surprisingly, accounting for partially drained conditions (including the change in pore water pressure) results in higher pile head moments, as negative excess pore water pressure significantly increases resistance. This is more pronounced for larger values of OCR_0. Very similar responses for jacked and WIP piles are observed for the initial phase of monotonic loading for both drainage conditions. However, at high values of rotation, the WIP piles exhibit lower resistance than the jacked piles. This is true for all values of OCR_0 and becomes even more evident for higher values of initial overconsolidation ratio. The larger OCR_0, the greater is the rotation at which the jacked piles and the WIP piles begin to diverge. These results indicate that the assumption of WIP conditions is conservative with respect to pile rotation and that the stiffness of the soil-pile system at small rotations, an important aspect for the design of offshore wind turbine foundations, is not significantly affected by the installation-related changes in soil state.

3.4 High-cyclic lateral loading following the installation

After the first and second step in which the vertical load is applied (see Section 3.3), the simulations with high-cyclic lateral loading are performed in the following steps:

3. Application of the average value of the moment M^{av} and the average value of the horizontal load H^{av}. Both the moment and the horizontal load are applied at the level of the seabed, see Fig. 7a. Depending on the initial value of OCR, different load magnitudes are studied. The considered loading scenarios are listed in Table 4. For each case, the ratio of the average value of moment M^{av} to the moment resistance M^R at a rotation of 2° for the jacked pile is given. M^R is obtained from the drained monotonic tests displayed in Fig. 8. The magnitudes of M^{av} and H^{av} are identical for both the jacked and WIP piles. This step is performed ideally drained, assuming that there is sufficient time for any excess pore water pressures caused by the average loading to dissipate before the cyclic loading starts.

4. Application of the first load cycle with a horizontal load amplitude $H^{\text{ampl}} = H^{\text{av}}$ and a moment amplitude of $M^{\text{ampl}} = M^{\text{av}}$ (see Table 4). This and all subsequent steps are carried out considering partially drained conditions, i.e. excess pore water pressures and consolidation processes. A frequency of 0.1 Hz for the cyclic loading is assumed.

5. Repetition of the previous step, recording the strain path at each integration point of each soil element of the model. The strain amplitude is calculated at the end of the step based on the recorded strain path.

6. Simulation of 10^6 additional load cycles using the HCA model, applying only the average load H^{av} and M^{av}. To simulate $N = 10^6$ cycles with a frequency of 0.1 Hz, a total time of 10^7 s is considered. The strain amplitude is updated in every 10th calculation increment. This corresponds to updates at $N \approx \{3,\ 5,\ 12,\ 30,\ 100,\ 300,\ 10^3,\ 3{\cdot}10^3,\ 10^4,\ 3{\cdot}10^4,\ 8{\cdot}10^4,\ 2{\cdot}10^5,\ 4{\cdot}10^5,\ 5{\cdot}10^5,\ 6{\cdot}10^5,\ 6{\cdot}10^5,\ 8{\cdot}10^5\}$. For a discussion of the importance of updating the strain amplitude and a more detailed explanation of the procedure, see Appendix A.

According to (DNV, 2021), the serviceability limit design needs to prove that the tilting at seabed resulting for a load level that is exceeded in 1 % of the lifetime of the structure is within a tolerable range. In addition, two other cases with a lower number of cycles need to be considered for which application of a high-cycle model is not mandatory and which are therefore not discussed further. Considering 25 years of operation, a load level that is exceeded in 1 % of the lifetime covers a time span of nearly 100 days (which is slightly less than 10^6 cycles with a duration of 10 s, being equivalent to approximately 115 days). In the simulations performed, this means that any load case resulting in a tilting exceeding $\theta = 0.25$ to $\theta = 0.5$ (depending if the tolerated tilting due to installation is included or not) at $N = 10^6$ is critical. Since the load is applied continuously in the simulations, without intermediate consolidation phases, the worst case scenario is modelled. Of course, the arrangement of cyclic loads for piles in water-saturated clay is an important influence (see e.g. the recent work reported in (Liu et al., 2022)), the further investigation of which is subject of future work.

For the first five steps, the MCC model and the parameters of "Karlsruhe kaolin" are used (see Table 1). Although the MCC model is not suitable for investigating cyclic loading in general, it is a sufficient model to calculate the strain amplitude required for the HCA model. This is because the model is not required to correctly describe cumulative effects. Even a simple fully elastic model would be sufficient to calculate the strain amplitude if the stiffness is properly defined. Due to its barotropic stiffness, the MCC model, unlike a simple elastic model, accounts for the influence of the mean effective stress on the strain amplitude.

The normalised horizontal pile head displacement u/D as a function of time for the simulations with an initial OCR of 1 is shown in the left-hand plot of Fig. 9 and for an initial OCR of 2 in the right-hand plot of Fig. 9 for the jacked and the WIP piles, respectively. Two different values for the moment $M^{\text{ampl}} = M^{\text{av}}$ (and thus the horizontal load $H^{\text{ampl}} = H^{\text{av}}$) are compared. In the simulation with $\text{OCR}_0 = 1$ and $M^{\text{ampl}} = M^{\text{av}} = 0.25$ MNm, the installation process influences both the short-term ($N \leq 10$) and the long-term ($N > 10$) response only insignificantly. However, the simulation taking into account the installation process leads to slightly larger pile head displacements in the long term. For the simulation with $\text{OCR}_0 = 1$ and $M^{\text{ampl}} = M^{\text{av}} = 0.5$ MNm, the assumption of WIP initial conditions leads to larger

OCR_0	$M^R(\theta = 2°)$ [MNm]	$M^{av} = M^{ampl}$ [MNm]	$M^{av}/M^R(\theta = 2°)$	$\theta(N = 10^5)$ WIP [°]	$\theta(N = 10^5)$ Jacking [°]
1	2.5	0.25	0.1	1.43	1.62
		0.5	0.2	> 3	> 3
2	4.2	0.25	0.06	0.5	0.22
		0.5	0.12	1.71	0.74
3	5.5	0.5	0.09	0.72	0.33
		0.75	0.14	1.57	0.65
6	6.5	0.75	0.12	0.3	0.29
		1.5	0.23	1.45	0.73

Table 4: Values of the average moment M^{av} and the amplitude of the moment M^{ampl} used for the analyses of the high-cyclic loading of the piles. Two different cases are considered for each initial value of OCR_0. The moment resistance M^R at a rotation of $\theta = 2°$ (see left-hand plot of Fig. 8) for the jacked piles and the corresponding ratio of M^{av}/M^R are given. In addition, the rotation at $N = 10^5$ for each loading scenario and different initial condition (WIP, jacking) is provided.

short- and long-term displacements. Very large values of pile head rotation are already reached at $N = 10^2$ (10^3 s), leading to non-convergence of the simulation.

A much larger influence of the installation process is found for an initial OCR value of 2, as can be seen from the right-hand plot of Fig. 9. While both jacked and WIP piles result in similar pile head displacements for both load magnitudes in the short-term, the WIP simulations predict much greater deformations in the long-term. This is more pronounced for the higher load magnitudes.

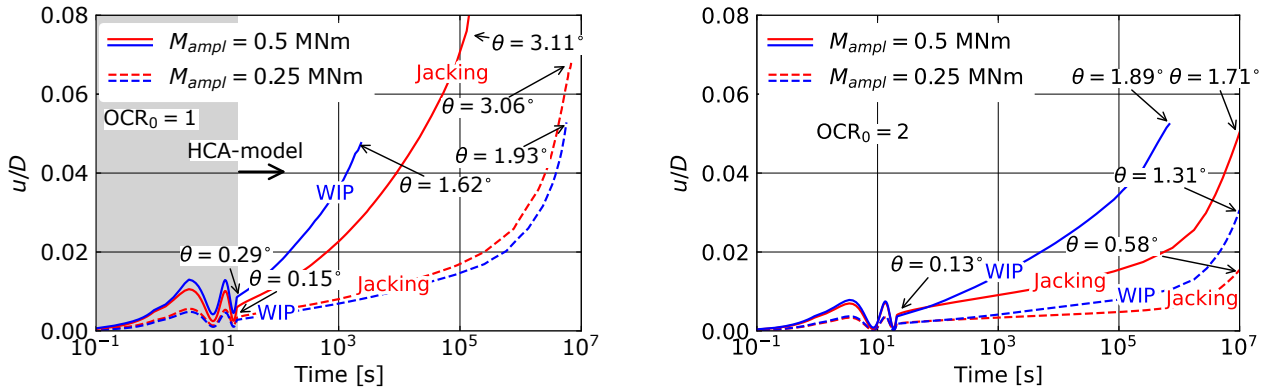

Figure 9: *Comparison of normalised horizontal displacement u/D vs. time plots of jacked and WIP piles for an initial OCR of 1 (left-hand plot) and 2 (right-hand plot). The load magnitudes are either $M^{ampl} = M^{av} = 0.5$ MNm and $H^{ampl} = H^{av} = 0.5/8$ MN (solid lines) or $M^{ampl} = M^{av} = 0.25$ MNm and $H^{ampl} = H^{av} = 0.25/8$ MN (dashed lines). The pile head rotation θ is given at $N = 2$ and at the end of the HCA phase.*

Very similar observations can be made for the simulations with $OCR_0 = 3$, as can be seen from the left-hand plot of Fig. 10. The omission of the installation process leads to significantly larger deformations in the long-term for both load magnitudes. In contrast to the simulation with $OCR_0 = 2$, however, the WIP simulations result in somewhat smaller deformations in the short-term ($N \leq 10$). This is also evident from the results of the simulation with an initial OCR of 6, given in the right-hand graph of Fig. 10. The WIP simulations result in lower pile head displacement up to $N = 10^2$ (10^3 s) for $M^{ampl} = M^{av} = 1.5$ MNm, but a much higher accumulation of deformations for larger number of load cycles. Similar but less pronounced tendencies are observed for the simulations with lower load magnitude. However, more load cycles are required before the WIP simulation shows larger deformations compared to the jacked pile.

Overall, the simulations show that the installation has a significant influence on the long-term behaviour of the pile, especially for overconsolidated soils. The assumption of WIP conditions tends to lead to higher accumulation rates and is therefore judged conservative with respect to the long-term cyclic behaviour of the pile. However, with increasing OCR, WIP conditions result in lower pile head displacements in the short term. Compared to the long-term cyclic behaviour, these differences between the two simulation types are smaller in the short-term. These tendencies are similar to those observed for monotonic loading, where only in case of large rotations significant differences between WIP and jacked piles were observed.

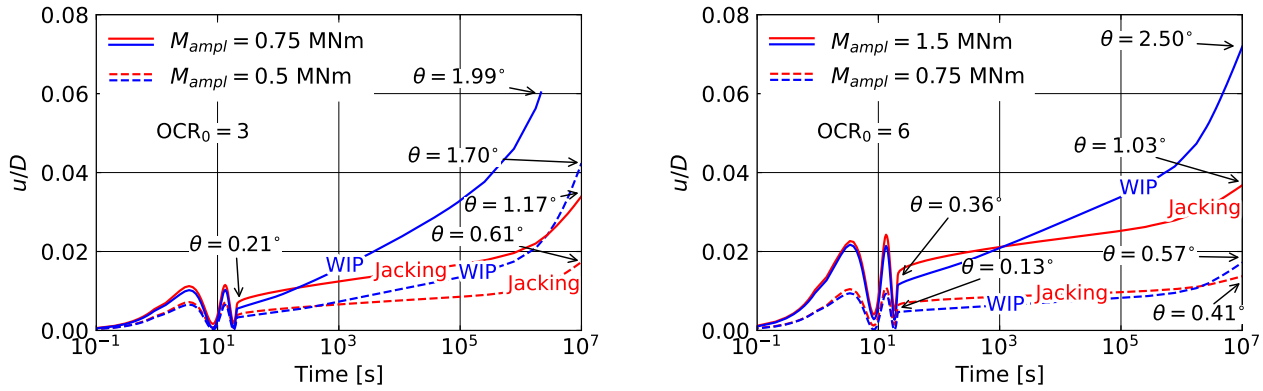

Figure 10: *Comparison of normalised horizontal displacement u/D vs. time plots of jacked and WIP piles for an initial OCR of 3 (left-hand plot) and 6 (right-hand plot). For $OCR_0 = 3$, the load magnitudes are either $M^{ampl} = M^{av} = 0.75$ MNm and $H^{ampl} = H^{av} = 0.75/8$ MN (solid lines) or $M^{ampl} = M^{av} = 0.5$ MNm and $H^{ampl} = H^{av} = 0.5/8$ MN (dashed lines). For $OCR_0 = 6$, the load magnitudes are either $M^{ampl} = M^{av} = 1.5$ MNm and $H^{ampl} = H^{av} = 1.5/8$ MN (solid lines) or $M^{ampl} = M^{av} = 0.75$ MNm and $H^{ampl} = H^{av} = 0.75/8$ MN (dashed lines). The pile head rotation θ is given at $N = 2$ and at the end of the HCA phase.*

To investigate by which effects the differences between the two simulation types are caused, the spatial distributions of the normalised mean effective stress (p/p_0) and OCR/OCR$_0$ at different times and numbers of cycles of the analyses, respectively, are given in Fig. 11a,b for the simulations with OCR$_0$ = 3. At $N = 2$, the mean effective stress in the case of the jacked pile is much higher at the pile tip and at the mean height of the pile compared to the WIP simulation. At $N = 10^5$, the mean effective stress is reduced significantly in the vicinity to the pile shaft for both analyses, but less for the jacked pile. At the same time, the spatial distribution of OCR shows much larger values around the pile shaft for the jacked pile as well. Since the mean effective stress at the outer pile shaft is initially larger in the case of the jacked pile, the potential increase in OCR is much larger with continued cyclic loading. Considering that the installation in clay with a higher initial OCR results in a large increase in effective stresses (see Fig. 4), but subsequent cyclic lateral loading results in a similarly large decrease in mean effective stresses, the OCR under cyclic lateral loading increases more for the jacked pile compared to the WIP simulation. This is underpinned by Fig. 12, which shows the time history of OCR/OCR$_0$, $\sigma_r/\sigma_{r,0}$ and p/p_0 for jacked and WIP piles. In case of the jacked pile, OCR tends to increase stronger with ongoing cyclic loading. This occurs despite a similarly large decrease in p/p_0, as explained before. Interestingly, Fig. 12 reveals that the change in $\sigma_r/\sigma_{r,0}$ is very different between the two simulations and a much lower reduction with increasing number of cycles is observed for the jacked pile. The decrease in p/p_0 for the jacked pile is predominantly a result from a decrease of the vertical and circumferential stress components. Such a decrease in mean effective stress under cyclic lateral loading of piles in clay is also frequently observed in experiments and field tests, resulting in a reduction in the stiffness of the soil-pile system (Puech and Garnier, 2017; Liao et al., 2018; Lai et al., 2020).

The spatial distributions of the strain amplitude at different numbers of load cycles are given in Fig. 13 for the jacked and WIP pile with OCR$_0$ = 3. As mentioned earlier, the strain amplitude is calculated from the second load cycle and updated several times during the high-cycle phase using the adaptive

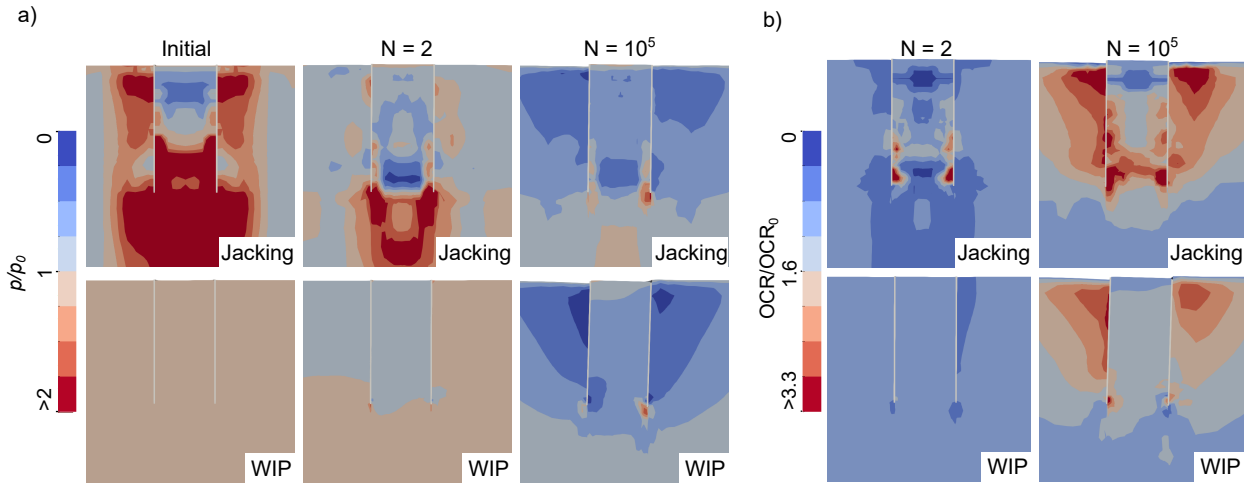

Figure 11: *a) Spatial distributions of normalised mean effective stress p/p_0 for jacked and WIP piles at different times of the analyses. b) Spatial distributions of OCR/OCR_0 for the same simulations at $N = 2$ and $N = 10^5$. The deformed configurations without a scale factor are displayed ($OCR_0 = 3$ and $M^{ampl} = M^{av} = 0.75$ MNm for both simulations).*

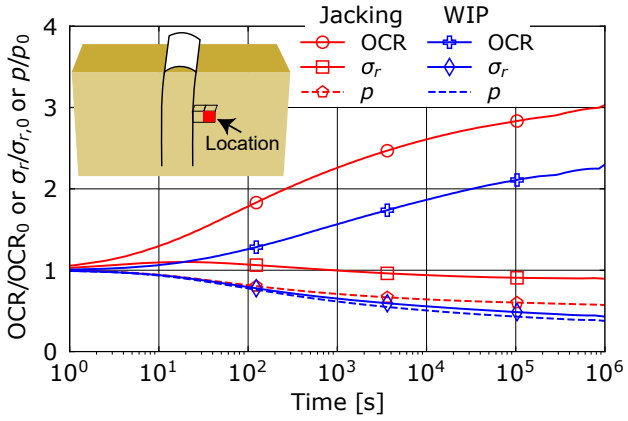

Figure 12: *Development of OCR/OCR_0, $\sigma_r/\sigma_{r,0}$ and p/p_0 for jacked and WIP piles at an element 4 m below the ground surface during the high-cycle phase ($OCR_0 = 3$ and $M^{ampl} = M^{av} = 0.75$ MNm for both simulations)*

strain amplitude definition. This definition takes into account the change in soil stiffness due to changes in effective stress and void ratio. Eq. (8) defines the soil stiffness as a function of the void ratio and the mean effective stress. Since both the mean effective stress and the void ratio decrease during the high-cyclic loading (see Fig. 11 for the mean effective stress), the stiffness decreases as well. This results in a continuous increase of the strain amplitude with increasing number of load cycles. In accordance with the spatial distribution of the normalised mean effective stress given in Fig. 11, the strain amplitude for the jacked pile increases less compared to the WIP simulation. This is especially the case in the lower third of the pile. Around the pile head, the differences in the change in strain amplitude are less pronounced, with both distributions being comparable at $N = 10^4$. Therefore, the large differences between the two simulation types in the long-term behaviour of the pile observed in the left-hand plot of Fig. 10 are not due to differences in strain amplitude, but to differences in OCR, as mentioned earlier.

The spatial distributions of the normalised excess pore water pressure $\Delta p^w/p_0^w$ (including the pressure from the free water table 10 m above the seabed) at different numbers of load cycles are given in Fig. 14 for $OCR_0 = 3$. The WIP simulation predicts a higher accumulation of excess pore water pressures compared to the jacked pile. This is most prominent for the soil below the pile tip, where the jacked pile shows initially much higher values of mean effective stress compared to the WIP simulation (see Fig. 11).

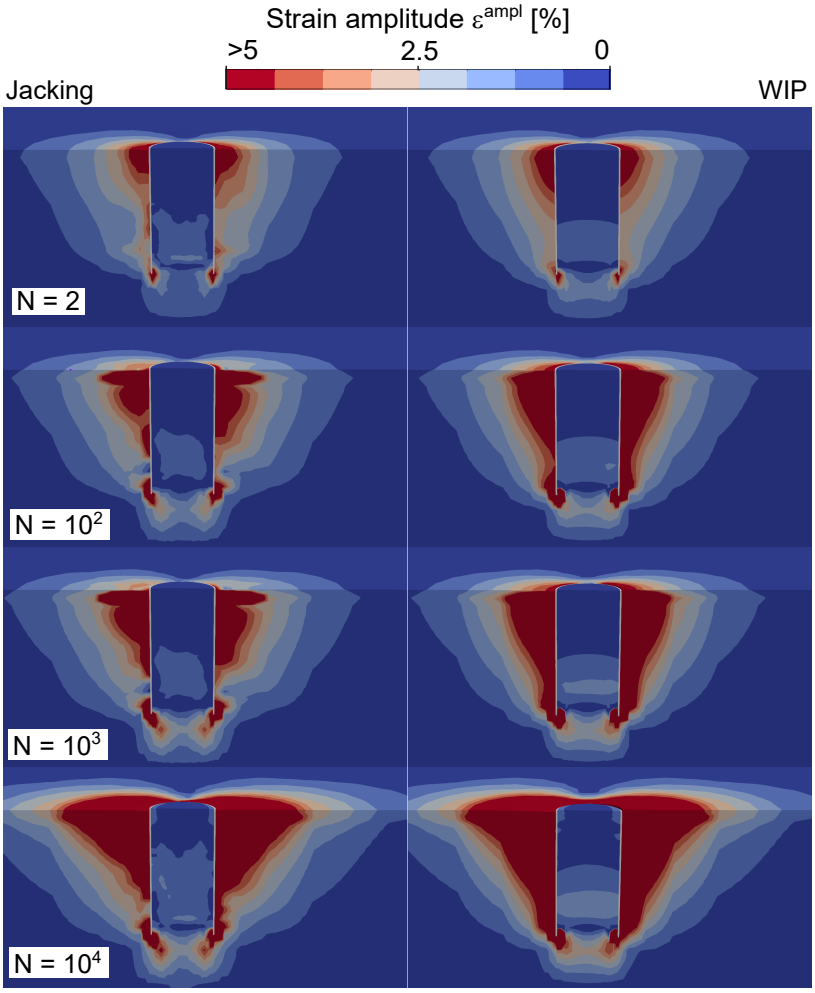

Figure 13: *Spatial distribution of the strain amplitude at different numbers of load cycles for the jacked and WIP pile with* $OCR_0 = 3$ *and* $M^{ampl} = M^{av} = 0.75$ *MNm. The deformed configurations without a scale factor are displayed.*

4 Conclusions

Simulations of the jacking process of large open-profile piles ($D = 4$ m) in clay were presented. Using the HCA model for clay, the piles were subsequently subjected to 10^6 lateral load cycles and the predicted pile deformations were compared with simulations neglecting the installation process. The following conclusions can be drawn from these investigations:

- The pile installation process in clay reduces the initial OCR values in overconsolidated soils considerably, in particular below the pile tip. Large values of negative excess pore water pressure are observed close to the pile shaft, which are larger at higher values of initial OCR. The effective radial stress increases significantly below the pile tip for initially overconsolidated soils, but much less for normally consolidated conditions. The h/R effect, i.e. the reduction in effective radial stress at the pile shaft with increasing pile penetration depth, is more pronounced at lower values of initial OCR, but much less than in sandy soils due to the aforementioned negative excess pore water pressures at the pile shaft.
- Cavitation can limit the pile resistance during installation and is important to be accounted for. This is more important for larger values of initial OCR.

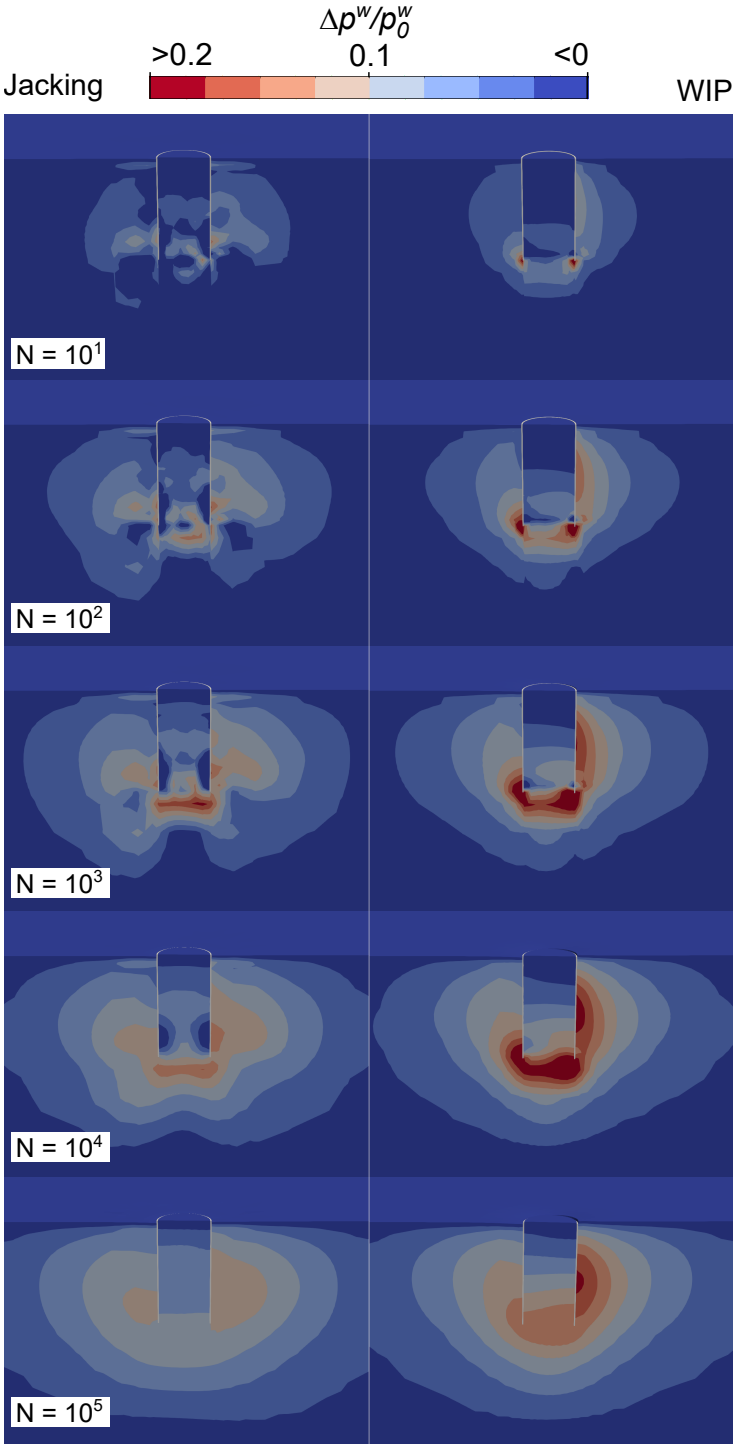

Figure 14: *Spatial distribution of the normalised excess pore water pressure* $\Delta p^w/p_0^w$ *at different numbers of load cycles for the jacked and WIP pile with* $OCR_0 = 3$ *and* $M^{ampl} = M^{av} = 0.75$ *MNm. The deformed configurations without a scale factor are displayed.*

- The consolidation process after installation leads to a decrease in effective stress near the pile shaft as negative excess pore water pressures dissipate in case of initially overconsolidated soils. At the same time, OCR increases, even at a greater distance from the pile shaft.
- Compared to the simulations neglecting the installation process, the monotonic lateral loading behaviour of jacked piles was found to be comparable for smaller values of pile head rotation. However, higher resistance was found for larger rotations in the simulations that considered the installation process. The greater the initial OCR prior to installation, the greater the rotation at which jacked and WIP piles began to diverge.
- When the pile was subjected to 10^6 lateral load cycles, simulations that neglected the installation process resulted in a much higher accumulation of lateral pile deformations for a larger number of load cycles ($N > 100$). This was especially pronounced for initially overconsolidated soils. For initially normally consolidated soils, installation did not change the pile response as much.
- With increasing initial OCR, neglecting the installation process resulted in lower pile deformations at a low number of load cycles ($N \leq 100$).
- The cyclic lateral loading after the consolidation process further reduced the effective stresses on the pile shaft while OCR increased. The increase in OCR is much more pronounced when the pile installation process is taken into account. This is particularly the case for initially overconsolidated soils, as the effective stress increased more during the installation process compared to normally consolidated initial conditions.

These results indicate that the practice of neglecting the installation process, i.e. assumption of wished-in-place conditions, is not necessarily justified. This is especially true for initially overconsolidated soils and a larger number of lateral load cycles, as is the case with piles in the offshore environment. However, in almost all cases investigated, neglecting the installation process resulted in slightly higher pile displacements and is therefore conservative.

Future work will focus on the application of more sophisticated constitutive models for the analysis of the pile installation process and the first two lateral loading cycles. In addition, different installation techniques could be investigated, since field tests have shown an influence of the installation method on the development of the decisive soil state variables during driving (Gavin et al., 2010).

Data availability statement

Some or all data, models, or code that support the findings of this study are available from the corresponding author upon reasonable request. `numgeo` can be freely downloaded from `www.numgeo.de`.

List of symbols

$\mathbf{1}$	second order unit tensor
$\boldsymbol{b}$	gravity vector
C_{ampl}	parameter of the HCA model in function f_{ampl}
C_e	parameter of the HCA model in function f_e
C_η	parameter of the HCA model in function f_η
C_{N1}	parameter of the HCA model in function f_N
C_{N2}	parameter of the HCA model in function f_N
C_{N3}	parameter of the HCA model in function f_N
C_{OCR}	parameter of the HCA model in function f_{OCR}
D	pile diameter
E	fourth order stiffness tensor
e^{av}	average void ratio
e_{ref}	reference void ratio
F	scalar value of yield surface
f	loading frequency
f_{ampl}	function of the HCA model considering the strain amplitude
f_e	function of the HCA model considering the void ratio
f_f	function of the HCA model considering the loading frequency
$\dot{f}_N$	function of the HCA model considering the cyclic history
$\dot{f}_N^A$	N-dependent function of the HCA model considering the cyclic history
$\dot{f}_N^B$	constant function of the HCA model considering the cyclic history
f_{OCR}	function of the HCA model considering the overconsolidation ratio
f_η	function of the HCA model considering the average stress ratio
G	scalar shear stiffness
g	gravity of earth
g^A	cyclic history state variable of the HCA model
$\dot{g}^A$	rate of the cyclic history state variable of the HCA model
H^{ampl}	amplitude of horizontal load
H^{av}	average horizontal load
H^w	height of water table above seabed
h	distance from the pile tip
I	fourth order unit tensor
I_P	plasticity index

I_v	viscosity index
K	bulk modulus of soil
K_0	lateral stress coefficient
K^{Perm}	permeability
K^w	bulk modulus of water
k^w	hydraulic conductivity of water
M	critical stress ratio
M^{ampl}	amplitude of moment
M^{av}	average moment
M^R	moment required for 2° rotation
M^{tot}	total moment applied at seabed level
$\mathbf{m}$	direction of accumulation
N	number of load cycles
n	porosity
OCR	overconsolidation ratio
$\mathrm{OCR}^{\mathrm{av}}$	average overconsolidation ratio
OCR_0	initial overconsolidation ratio
p_{atm}	atmospheric pressure
p^{av}	average mean effective stress
p_e^+	average equivalent mean effective stress for $F = 0$
p_e^{av}	average equivalent mean effective stress
p^w	pore water pressure
p_0^w	initial pore water pressure
$\dot{p}^w$	rate of pore water pressure
q^{av}	average deviatoric stress
R	pile radius
r	radial distance from pile shaft
t	physical time
t_{cycle}	duration of a single cycle
u	horizontal pile head displacement
$\dot{\boldsymbol{u}}^s$	velocity of the solid phase
$\ddot{\boldsymbol{u}}^s$	acceleration of the solid phase
w_L	liquid limit

Δp^w	excess pore water pressure
Δt	time increment
$\dot{\boldsymbol{\varepsilon}}$	strain rate
$\dot{\boldsymbol{\varepsilon}}^{\mathrm{acc}}$	strain accumulation rate
$\varepsilon^{\mathrm{ampl}}$	strain amplitude
$\varepsilon^{\mathrm{ampl}}_{\mathrm{ref}}$	reference strain amplitude
$\dot{\boldsymbol{\varepsilon}}^{\mathrm{pl}}$	plastic strain rate
η^{av}	average stress ratio
η^w	dynamic viscosity of water
θ	pile head rotation
κ	swelling index
λ	compression index
μ	friction coefficient
ν	Poisson's ratio
ρ^w	water density
$\boldsymbol{\sigma}$	effective stress
$\mathring{\boldsymbol{\sigma}}$	objective effective stress rate
σ_r	effective radial stress
$\sigma_{r,0}$	initial effective radial stress
$\boldsymbol{\sigma}^{\mathrm{av}}$	average effective stress
$(\boldsymbol{\sigma}^{\mathrm{av}})^*$	deviatoric average effective stress
φ_c	critical friction angle

A Update of the strain amplitude using the adaptive strain amplitude definition

The adaptive strain amplitude definition proposed in (Staubach et al., 2022a) is used to account for the influence of the change in soil stiffness during the high-cycle phase on the strain amplitude calculated from the second load cycle. The significance of updating the strain amplitude is discussed in the following. Figure 15 shows the normalised horizontal displacement u/D of jacked piles with an initial OCR of 3 assuming a constant strain amplitude during the high-cycle phase (*const.* $\varepsilon^{\text{ampl}}$) or using the adaptive strain amplitude definition ($\varepsilon^{\text{ampl}}(N)$). As explained in Section 3.4, the strain amplitude is updated every 10th calculation increment during the high-cycle phase, giving a total of almost 20 updates. As explained in (Staubach et al., 2022a), the spatial distribution of the strain amplitude is smoothed after the update by a nonlocal smoothing algorithm. The characteristic length l_c, which influences the number and the weighting of the neighbouring integration points considered in the smoothing of the strain amplitude field, is set to 1 m. In (Staubach et al., 2022a) it was demonstrated that for similar pile specifications as considered here, $l_c = 1$ m is an appropriate choice.

Figure 15 shows that the assumption of a constant strain amplitude up to $N = 10^4$ (10^5 s) is justified, but leads to a much smaller accumulation of permanent pile head displacements for a larger number of load cycles. This is consistent with the spatial distribution of the strain amplitude given in Fig. 13, which shows the largest increase from $N = 10^3$ to $N = 10^4$. As explained earlier, the increase in strain amplitude is due to the decrease in mean effective stress and void ratio during the high-cyclic loading, which leads to a decrease in soil stiffness (and hence in stiffness of the soil-pile system as well). Figure 15 demonstrates that the assumption of a constant strain amplitude is not conservative, especially for a larger number of load cycles. Therefore, updating the strain amplitude for the HCA model for clay is considered mandatory when a large number of load cycles must be considered.

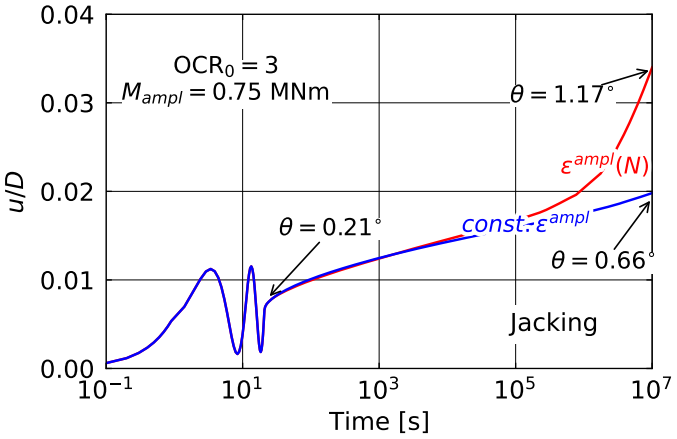

Figure 15: *Comparison of normalised horizontal displacement u/D vs. time plots of jacked piles for an initial OCR of 3 assuming a constant strain amplitude during the high-cycle phase (const. $\varepsilon^{\text{ampl}}$) or using the adaptive strain amplitude definition ($\varepsilon^{\text{ampl}}(N)$). The load magnitudes are $M^{\text{ampl}} = M^{\text{av}} = 0.75$ MNm and $H^{\text{ampl}} = H^{\text{av}} = 0.75/8$ MN.*

References

Ali, A., T. Meier, and I. Herle (2011). "Numerical investigation of undrained cavity expansion in fine-grained soils". In: *Acta Geotechnica* 6.1, pp. 31–40. ISSN: 18611133.

Aubram, D., F. Rackwitz, P. Wriggers, and S. A. Savidis (Apr. 2015). "An ALE method for penetration into sand utilizing optimization-based mesh motion". In: *Computers and Geotechnics* 65, pp. 241–249. ISSN: 18737633.

Baligh, M. (Sept. 1985). "Strain Path Method". In: *Journal of Geotechnical Engineering* 111.9, pp. 1108–1136. URL: https://doi.org/10.1061/(ASCE)0733-9410(1985)111:9(1108).

Benson, D. J. (1992). "Computational methods in Lagrangian and Eulerian hydrocodes". In: *Computer Methods in Applied Mechanics and Engineering* 99.2, pp. 235–394. ISSN: 0045-7825.

Benson, D. J. and S. Okazawa (2004). "Contact in a multi-material Eulerian finite element formulation". In: *Computer Methods in Applied Mechanics and Engineering* 193.39, pp. 4277–4298. ISSN: 0045-7825.

Bienen, B., S. Fan, M. Schröder, and M. F. Randolph (Sept. 2021). "Effect of the installation process on monopile lateral response". In: *Proceedings of the Institution of Civil Engineers - Geotechnical Engineering*, pp. 1–19. ISSN: 1353-2618. URL: https://doi.org/10.1680/jgeen.20.00219%20https://www.icevirtuallibrary.com/doi/10.1680/jgeen.20.00219.

Bond, A. J. and R. J. Jardine (1991). "Effects of installing displacement piles in a high OCR clay". In: *Geotechnique* 41.3, pp. 341–363. ISSN: 17517656. URL: https://doi.org/10.1680/geot.1991.41.3.341.

Borja, R. I. and S. R. Lee (Jan. 1990). "Cam-Clay plasticity, Part 1: Implicit integration of elasto-plastic constitutive relations". In: *Computer Methods in Applied Mechanics and Engineering* 78.1, pp. 49–72. ISSN: 00457825. URL: https://linkinghub.elsevier.com/retrieve/pii/004578259090152C.

Chen, F., L. Liu, F. Lai, K. Gavin, K. N. Flynn, and Y. Li (2022). "Numerical analyses of energy balance and installation mechanisms of large-diameter tapered monopiles by impact driving". In: *Ocean Engineering* 266, p. 113017. ISSN: 0029-8018. URL: https://www.sciencedirect.com/science/article/pii/S0029801822023009.

Coop, M. R. and C. P. Wroth (1989). "Field studies of an instrumented model pile in clay". In: *Geotechnique* 39.4, pp. 679–696. ISSN: 00168505. URL: https://doi.org/10.1680/geot.1989.39.4.679.

Cui, J., J. Li, and G. Zhao (2019). "Long-term time-dependent load-settlement characteristics of a driven pile in clay". In: *Computers and Geotechnics* 112, pp. 41–50. ISSN: 0266-352X. URL: https://www.sciencedirect.com/science/article/pii/S0266352X19301107.

De Chaunac, H. and A. Holeyman (2018). "Numerical analysis of the set-up around the shaft of a closed-ended pile driven in clay". In: *Geotechnique* 68.4, pp. 332–344. ISSN: 17517656. URL: https://doi.org/10.1680/jgeot.16.P.229.

DNV (2021). *DNV-ST-0126*.

Doherty, P. and K. Gavin (Nov. 2011). "Shaft Capacity of Open-Ended Piles in Clay". In: *Journal of Geotechnical and Geoenvironmental Engineering* 137.11, pp. 1090–1102. ISSN: 1090-0241. URL: https://doi.org/10.1061/(ASCE)GT.1943-5606.0000528%20http://ascelibrary.org/doi/10.1061/%7B%5C%%7D28ASCE%7B%5C%%7D29GT.1943-5606.0000528.

Duque, J., M. Ochmański, D. Mašín, Y. Hong, and L. Wang (June 2021). "On the behavior of monopiles subjected to multiple episodes of cyclic loading and reconsolidation in cohesive soils". In: *Computers and Geotechnics* 134, p. 104049. ISSN: 0266352X. URL: https://linkinghub.elsevier.com/retrieve/pii/S0266352X21000525.

Dyson, G. J. and M. F. Randolph (2001). "Monotonic Lateral Loading of Piles in Calcareous Sand". In: *Journal of Geotechnical and Geoenvironmental Engineering* 127.4, pp. 346–352.

Ehlers, W. and J. Bluhm (2013). *Porous Media: Theory, Experiments and Numerical Applications*. Springer Berlin Heidelberg. ISBN: 9783662049990. URL: https://books.google.de/books?id=vbXoCAAAQBAJ.

Engin, H. K., R. B. J. Brinkgreve, and A. F. van Tol (Oct. 2015). "Simplified numerical modelling of pile penetration - the press-replace technique". In: *International Journal for Numerical and Analytical Methods in Geomechanics* 39.15, pp. 1713–1734. ISSN: 0363-9061. URL: https://doi.org/10.1002/nag.2376.

Fan, S., B. Bienen, and M. F. Randolph (May 2021a). "Effects of Monopile Installation on Subsequent Lateral Response in Sand. II: Lateral Loading". In: *Journal of Geotechnical and Geoenvironmental Engineering* 147.5, p. 04021022. ISSN: 1090-0241. URL: http://ascelibrary.org/doi/10.1061/%7B%5C%%7D28ASCE%7B%5C%%7D29GT.1943-5606.0002504.

Fan, S., B. Bienen, and M. F. Randolph (2021b). "Centrifuge study on effect of installation method on lateral response of monopiles in sand". In: *International Journal of Physical Modelling in Geotechnics* 21.1, pp. 40–52. ISSN: 20426550.

Fan, S., B. Bienen, and M. F. Randolph (2021c). "Effects of Monopile Installation on Subsequent Lateral Response in Sand. I: Pile Installation". In: *Journal of Geotechnical and Geoenvironmental Engineering* 147.5, p. 04021021. ISSN: 1090-0241.

Gavin, K., D. Gallagher, P. Doherty, and B. McCabe (June 2010). "Field investigation of the effect of installation method on the shaft resistance of piles in clay". In: *Canadian Geotechnical Journal* 47.7, pp. 730–741. ISSN: 0008-3674. URL: https://doi.org/10.1139/T09-146.

Gong, W., L. Li, S. Zhang, and J. Li (2020). "Long-term setup of a displacement pile in clay: An analytical framework". In: *Ocean Engineering* 218, p. 108143. ISSN: 0029-8018. URL: https://www.sciencedirect.com/science/article/pii/S0029801820310805.

Hamann, T. (2015). "Zur Modellierung wassergesättigter Böden unter dynamischer Belastung und großen Bodenverformungen am Beispiel der Pfahleinbringung". PhD thesis. Publications of the Institute of Geotechnical Engineering and Construction Management, University of Hamburg.

Hamann, T., G. Qiu, and J. Grabe (2015). "Application of a Coupled Eulerian-Lagrangian approach on pile installation problems under partially drained conditions". In: *Computers and Geotechnics* 63, pp. 279–290. ISSN: 0266-352X.

Hauser, L. and H. F. Schweiger (2021). "Numerical study on undrained cone penetration in structured soil using G-PFEM". In: *Computers and Geotechnics* 133, p. 104061. ISSN: 18737633. URL: https://www.sciencedirect.com/science/article/pii/S0266352X21000653.

Heins, E. and J. Grabe (2017). "Class-A-prediction of lateral pile deformation with respect to vibratory and impact pile driving". In: *Computers and Geotechnics* 86, pp. 108–119. ISSN: 18737633.

Hong, Y., B. He, L. Z. Wang, Z. Wang, C. W. Ng, and D. Mašín (2017). "Cyclic lateral response and failure mechanisms of semi-rigid pile in soft clay: Centrifuge tests and numerical modelling". In: *Canadian Geotechnical Journal* 54.6, pp. 806–824. ISSN: 12086010.

Hughes, T. J. and J. Winget (1980). "Finite rotation effects in numerical integration of rate constitutive equations arising in large deformation analysis". In: *International Journal for Numerical Methods in Engineering* 15.12, pp. 1862–1867. ISSN: 10970207.

Jardine, R. J., B. T. Zhu, P. Foray, and Z. X. Yang (2013). "Interpretation of stress measurements made around closed-ended displacement piles in sand". In: *Geotechnique* 63.8, pp. 613–627. ISSN: 00168505.

Jostad, H. P., B. M. Dahl, A. Page, N. Sivasithamparam, and H. Sturm (2020). "Evaluation of soil models for improved design of offshore wind turbine foundations in dense sand". In: *Geotechnique* 70.8, pp. 682–699. ISSN: 17517656.

Karlsrud, K. and T. Haugen (1986). "Axial Static Capacity of Steel Model Piles in Overconsolidated Clay." In: *Publikasjon - Norges Geotekniske Institutt*. 163. Rotterdam, pp. 1401–1406. ISBN: 8254601275.

Klinkvort, R. T. (2013). "Centrifuge modelling of drained lateral pile - soil response: Application for offshore wind turbine support structures". PhD thesis. ISBN: 9788778773579.

Kong, D., J. Zhu, Y. Long, B. Zhu, Q. Yang, Y. Gao, and Y. Chen (2022). "Centrifuge modelling on monotonic and cyclic lateral behaviour of monopiles in kaolin clay". In: *Géotechnique* 0.0, pp. 1–14. URL: https://doi.org/10.1680/jgeot.19.P.402.

Lacal-Arántegui, R., J. M. Yusta, and J. A. Domínguez-Navarro (2018). "Offshore wind installation: Analysing the evidence behind improvements in installation time". In: *Renewable and Sustainable Energy Reviews* 92, pp. 133–145. ISSN: 1364-0321. URL: https://www.sciencedirect.com/science/article/pii/S1364032118302612.

Lai, Y., L. Wang, Y. Hong, and B. He (2020). "Centrifuge modeling of the cyclic lateral behavior of large-diameter monopiles in soft clay: Effects of episodic cycling and reconsolidation". In: *Ocean Engineering* 200, p. 107048. ISSN: 00298018.

Le, V. H., F. Remspecher, and F. Rackwitz (2021). "Development of numerical models for the long-term behaviour of monopile foundations under cyclic loading considering the installation effects". In: *Soil Dynamics and Earthquake Engineering* 150, p. 106927. ISSN: 02677261. URL: https://www.sciencedirect.com/science/article/pii/S0267726121003493.

Lehane, B. M. and D. R. Gill (2004). "Displacement fields induced by penetrometer installation in an artificial soil". In: *International Journal of Physical Modelling in Geotechnics* 4.1, pp. 25–36. URL: https://doi.org/10.1680/ijpmg.2004.040103.

Lehane, B. M. and R. J. Jardine (1994a). "Displacement pile behaviour in glacial clay". In: *Canadian Geotechnical Journal* 31.1, pp. 79–90. ISSN: 00083674. URL: https://doi.org/10.1139/t94-009.

Lehane, B. M. and R. J. Jardine (1994b). "Displacement-pile behaviour in a soft marine clay". In: *Canadian Geotechnical Journal* 31.2, pp. 181–191. ISSN: 00083674. URL: https://doi.org/10.1139/t94-024.

Lehane, B. M., C. O'Loughlin, C. Gaudin, and M. F. Randolph (2009). "Rate effects on penetrometer resistance in kaolin". In: *Géotechnique* 59.1, pp. 41–52. URL: https://doi.org/10.1680/geot.2007.00072.

Li, Q., K. Gavin, A. Askarinejad, and L. J. Prendergast (July 2021). "Experimental and numerical investigation of the effect of vertical loading on the lateral behaviour of monopiles in sand". In: *Canadian Geotechnical Journal*. ISSN: 0008-3674. URL: https://doi.org/10.1139/cgj-2020-0769.

Liao, W., J. Zhang, J. Wu, and K. Yan (2018). "Response of flexible monopile in marine clay under cyclic lateral load". In: *Ocean Engineering* 147, pp. 89–106. ISSN: 00298018. URL: http://www.sciencedirect.com/science/article/pii/S0029801817306248.

Lin, C., J. Han, C. Bennett, and R. L. Parsons (2016). "Analysis of laterally loaded piles in soft clay considering scour-hole dimensions". In: *Ocean Engineering* 111, pp. 461–470. ISSN: 0029-8018. URL: https://www.sciencedirect.com/science/article/pii/S0029801815006514.

Liu, H., N. Sivasithamparam, Y. Suzuki, and H. P. Jostad (2022). "Load history idealisation effects for design of monopiles in clay". In: *Géotechnique*. URL: https://doi.org/10.1680/jgeot.22.00010.

Machaček, J. and P. Staubach (2021). "numgeo: A finite-element program for the simulation of hydro-mechanically coupled geotechnical processes". In: *Fachsektionstage Geotechnik 2021*. DGGT. URL: https://www.numgeo.de/wp-content/uploads/2022/01/numgeoMachacekStaubachFSTB2021.pdf.

Machaček, J., P. Staubach, M. Tafili, H. Zachert, and T. Wichtmann (2021). "Investigation of three sophisticated constitutive soil models: From numerical formulations to element tests and the analysis of vibratory pile driving tests". In: *Computers and Geotechnics* 138, p. 104276. ISSN: 18737633.

Machaček, J. (2020). *Contributions to the Numerical Modelling of Saturated and Unsaturated Soils*. Dissertation, Publications of the Institute of Soil Mechanics and Rock Mechanics, Karlsruhe Institute of Technology, Issue No. 187.

Matsuoka, H. and T. Nakai (1974). "Stress-Deformation and Strength Characteristics of Soil Under Three Different Principal Stresses." In: *Proc Jap Soc Civ Eng*. Vol. 1974. 232. Japan Society of Civil Engineers, pp. 59–70.

Mayne, P. and F. H. Kulhawy (1982). "K-OCR relationships in soil". In: *Journal of Geotechnical Engineering* 108, pp. 851–872.

Mita, K. A., G. R. Dasari, and K. W. Lo (Dec. 2004). "Performance of a Three-Dimensional Hvorslev-Modified Cam Clay Model for Overconsolidated Clay". In: *International Journal of Geomechanics* 4.4, pp. 296–309. URL: https://doi.org/10.1061/(ASCE)1532-3641(2004)4:4(296).

Monforte, L., M. Arroyo, J. M. Carbonell, and A. Gens (2018). "Coupled effective stress analysis of insertion problems in geotechnics with the Particle Finite Element Method". In: *Computers and Geotechnics* 101, pp. 114–129. ISSN: 18737633. URL: https://www.sciencedirect.com/science/article/pii/S0266352X18300909.

Ni, Q., C. C. Hird, and I. Guymer (2010). "Physical modelling of pile penetration in clay using transparent soil and particle image velocimetry". In: *Géotechnique* 60.2, pp. 121–132. URL: https://doi.org/10.1680/geot.8.P.052.

Niemunis, A., T. Wichtmann, and T. Triantafyllidis (2005). "A high-cycle accumulation model for sand". In: *Computers and Geotechnics* 32.4, pp. 245–263.

Page, A. M., G. Grimstad, G. Eiksund, and H. Jostad (2018). "A macro-element pile foundation model for integrated analyses of monopile-based offshore wind turbines". In: *Ocean Engineering* 167, pp. 23–35. ISSN: 0029-8018.

Page, A. M., R. T. Klinkvort, S. Bayton, Y. Zhang, and H. P. Jostad (Jan. 2021). "A procedure for predicting the permanent rotation of monopiles in sand supporting offshore wind turbines". In: *Marine Structures* 75, p. 102813. ISSN: 09518339. URL: https://linkinghub.elsevier.com/retrieve/pii/S0951833920301076.

Puech, A. and J. Garnier (2017). "Behavior of Piles Subject to Cyclic Lateral Loading". In: *Design of Piles Under Cyclic Loading*. John Wiley & Sons, Ltd. Chap. 8, pp. 233–297. ISBN: 9781119469018.

Qiu, G., S. Henke, and J. Grabe (2011). "Application of a Coupled Eulerian-Lagrangian Approach on Geomechanical Problems Involving Large Deformation". In: *Computers and Geotechnics* 38, pp. 30–39.

Randolph, M. F. (Dec. 2003). "Science and empiricism in pile foundation design". In: *Géotechnique* 53.10, pp. 847–875. ISSN: 0016-8505. URL: https://www.icevirtuallibrary.com/doi/10.1680/geot.2003.53.10.847.

Randolph, M. F., J. P. Carter, and C. P. Wroth (1979). "Driven piles in clay-the effects of installation and subsequent consolidation". In: *Géotechnique* 29.4, pp. 361–393. URL: https://doi.org/10.1680/geot.1979.29.4.361.

Rezania, M., M. Mousavi Nezhad, H. Zanganeh, J. Castro, and N. Sivasithamparam (Mar. 2017). "Modeling Pile Setup in Natural Clay Deposit Considering Soil Anisotropy, Structure, and Creep Effects: Case Study". In: *International Journal of Geomechanics* 17.3, p. 04016075. ISSN: 1532-3641. URL: https://doi.org/10.1061/(ASCE)GM.1943-5622.0000774%20http://ascelibrary.org/doi/10.1061/%7B%5C%%7D28ASCE%7B%5C%%7D29GM.1943-5622.0000774.

Roscoe, K. H. and J. B. Burland (1968). "On the generalized stress-strain behaviour of wet clays". In: *Engineering plasticity*. Ed. by J. Heyman and F. A. Leckie. Cambridge University Press, pp. 535–609.

Sagaseta, C., A. J. Whittle, and M. Santagata (Oct. 1997). "Deformation analysis of shallow penetration in clay". In: *International Journal for Numerical and Analytical Methods in Geomechanics* 21.10, pp. 687–719. ISSN: 0363-9061. URL: https://www.deepdyve.com/lp/wiley/deformation-analysis-of-shallow-penetration-in-clay-cN507tVUau%20https://onlinelibrary.wiley.com/doi/10.1002/(SICI)1096-9853(199710)21:10%7B%5C%%7D3C687::AID-NAG897%7B%5C%%7D3E3.0.CO;2-3.

Sheng, D., K. D. Eigenbrod, and P. Wriggers (2005). "Finite element analysis of pile installation using large-slip frictional contact". In: *Computers and Geotechnics* 32.1, pp. 17–26. ISSN: 0266-352X. URL: https://www.sciencedirect.com/science/article/pii/S0266352X04001326.

Silva, M. F., D. J. White, and M. D. Bolton (2006). "An analytical study of the effect of penetration rate on piezocone tests in clay". In: 30.6, pp. 501–527. URL: https://onlinelibrary.wiley.com/doi/abs/10.1002/nag.490.

Staubach, P. and J. Machaček (Aug. 2019). "Influence of relative acceleration in saturated sand: Analytical approach and simulation of vibratory pile driving tests". In: *Computers and Geotechnics* 112, pp. 173–184. ISSN: 0266352X. URL: https://linkinghub.elsevier.com/retrieve/pii/S0266352X19301028.

Staubach, P., J. Machaček, R. Sharif, and T. Wichtmann (June 2021a). "Back-analysis of model tests on piles in sand subjected to long-term lateral cyclic loading: Impact of the pile installation and application of the HCA model". In: *Computers and Geotechnics* 134, p. 104018. ISSN: 0266352X. URL: https://linkinghub.elsevier.com/retrieve/pii/S0266352X21000215.

Staubach, P., J. Machaček, M. C. Moscoso, and T. Wichtmann (2020). "Impact of the installation on the long-term cyclic behaviour of piles in sand: A numerical study". In: *Soil Dynamics and Earthquake Engineering* 138, p. 106223. ISSN: 02677261.

Staubach, P., J. Machaček, J. Skowronek, and T. Wichtmann (Feb. 2021b). "Vibratory pile driving in water-saturated sand: Back-analysis of model tests using a hydro-mechanically coupled CEL method". In: *Soils and Foundations* 61.1, pp. 144–159. ISSN: 00380806.

Staubach, P., J. Machaček, L. Tschirschky, and T. Wichtmann (Feb. 2022a). "Enhancement of a high-cycle accumulation model by an adaptive strain amplitude and its application to monopile foundations". In: *International Journal for Numerical and Analytical Methods in Geomechanics* 46.2, pp. 315–338. ISSN: 0363-9061. URL: https://onlinelibrary.wiley.com/doi/10.1002/nag.3301.

Staubach, P., J. Machaček, M. Tafili, and T. Wichtmann (Mar. 2022b). "A high-cycle accumulation model for clay and its application to monopile foundations". In: *Acta Geotechnica* 17.3, pp. 677–698. ISSN:

1861-1125. URL: 10.1007/s11440-021-01446-9%20https://link.springer.com/10.1007/s11440-021-01446-9.
Staubach, P., J. Machaček, and T. Wichtmann (Dec. 2021c). "Large-deformation analysis of pile installation with subsequent lateral loading: Sanisand vs. Hypoplasticity". In: *Soil Dynamics and Earthquake Engineering* 151, p. 106964. ISSN: 02677261. URL: https://linkinghub.elsevier.com/retrieve/pii/S0267726121003869.
Staubach, P., J. Machaček, and T. Wichtmann (May 2022c). "Novel approach to apply existing constitutive soil models to the modelling of interfaces". In: *International Journal for Numerical and Analytical Methods in Geomechanics* 46.7, pp. 1241–1271. ISSN: 0363-9061. URL: https://onlinelibrary.wiley.com/doi/10.1002/nag.3344.
Taylor, C. and P. Hood (1973). "A numerical solution of the Navier-Stokes equations using the finite element technique". In: *Computers and Fluids* 1.1, pp. 73–100. ISSN: 00457930. URL: https://www.sciencedirect.com/science/article/pii/0045793073900273.
Truong, P. and B. M. Lehane (2018). "Effects of pile shape and pile end condition on the lateral response of displacement piles in soft clay". In: *Géotechnique* 68.9, pp. 794–804. URL: https://doi.org/10.1680/jgeot.16.P.291.
Waltz, J. (2013). "Operator splitting and time accuracy in Lagrange plus remap solution methods". In: *Journal of Computational Physics* 253, pp. 247–258. ISSN: 0021-9991.
White, D. J. and M. D. Bolton (2004). "Displacement and strain paths during plane-strain model pile installation in sand". In: *Géotechnique* 54.6, pp. 375–397.
White, D. J. and B. M. Lehane (2004). "Friction fatigue on displacement piles in sand". In: *Geotechnique* 54.10, pp. 645–658. ISSN: 00168505.
Wichtmann, T. (2016). *Soil Behaviour Under Cyclic Loading: Experimental Observations, Constitutive Description and Applications*. Habilitation, Institute of Soil Mechanics and Rock Mechanics, Karlsruhe Institute of Technology, Issue No. 181.
Wichtmann, T. and T. Triantafyllidis (2018). "Monotonic and cyclic tests on Kaolin - a database for the development, calibration and verification of constitutive models for cohesive soils with focus to cyclic loading". In: *Acta Geotechnica* 13.5, pp. 1103–1128.
Xu, X. T., H. L. Liu, and B. M. Lehane (Oct. 2006). "Pipe pile installation effects in soft clay". In: *Proceedings of the Institution of Civil Engineers - Geotechnical Engineering* 159.4, pp. 285–296. ISSN: 1353-2618. URL: https://doi.org/10.1680/geng.2006.159.4.285%20https://www.icevirtuallibrary.com/doi/10.1680/geng.2006.159.4.285.
Yang, Q., Y. Gao, D. Kong, and B. Zhu (2019). "Centrifuge modelling of lateral loading behaviour of a semi-rigid Monopile in soft clay". In: *Marine Georesources and Geotechnology* 37.10, pp. 1205–1216. ISSN: 15210618.
Yang, Z. X., Y. Y. Gao, R. J. Jardine, W. B. Guo, and D. Wang (2020). "Large Deformation Finite-Element Simulation of Displacement-Pile Installation Experiments in Sand". In: *Journal of Geotechnical and Geoenvironmental Engineering* 146.6, p. 4020044.
Zachert, H., T. Wichtmann, P. Kudella, T. Triantafyllidis, and U. Hartwig (2020). "Inspection of a high-cycle accumulation model for sand based on recalculations of a full-scale test on a gravity base foundation for offshore wind turbines". In: *Computers and Geotechnics* 126.10, p. 103727.
Zdravkovic, L. et al. (2020). "Finite-element modelling of laterally loaded piles in a stiff glacial clay till at Cowden". In: *Geotechnique* 70.11, pp. 999–1013. ISSN: 17517656. URL: https://doi.org/10.1680/jgeot.18.PISA.005.
Zhang, W., J. qiang Zou, X. wei Zhang, W. hai Yuan, and W. Wu (Aug. 2021). "Interpretation of cone penetration test in clay with smoothed particle finite element method". In: *Acta Geotechnica* 16.8, pp. 2593–2607. ISSN: 18611133. URL: https://doi.org/10.1007/s11440-021-01217-6%20https://link.springer.com/10.1007/s11440-021-01217-6.
Zienkiewicz, O. C., C. T. Chang, and P. Bettess (1980). "Drained, undrained, consolidating and dynamic behaviour assumptions in soils". In: *Geotechnique* 30.4, pp. 385–395.